SIMULATION SOFTWARE FOR A HUMAN VENTRICULAR MYOCYTE MODEL

by

Ömer OYLAR

B.S. in Electronics Engineering, Uludağ University, 2012

Submitted to the Institute of Biomedical Engineering
in partial fulfillment of the requirements
for the degree of
Master of Science
in
Biomedical Engineering

Boğaziçi University
2019

SIMULATION SOFTWARE FOR A HUMAN VENTRICULAR MYOCYTE MODEL

APPROVED BY:

Assoc. Prof. Dr. Özgür KOCATÜRK .....
(Thesis Advisor)

Prof. Dr. Hale SAYBAŞILI .....

Assist. Prof. Dr. Ceyhun KIRIMLI .....

DATE OF APPROVAL: 20 June 2019

ACKNOWLEDGMENTS

I would like to convey my special thanks and appreciation to my thesis advisor, Assoc. Prof. Dr. Özgür Kocatürk for his continuous and friendly guidance during my master's study and the thesis.

I would like to express my deepest thanks to my family for their endless support, encouragement, and patience.

ACADEMIC ETHICS AND INTEGRITY STATEMENT

I, Ömer Oylar, hereby certify that I am aware of the Academic Ethics and Integrity Policy issued by the Council of Higher Education (YÖK) and I fully acknowledge all the consequences due to its violation by plagiarism or any other way.

Name :

Signature:

Date:

ABSTRACT

SIMULATION SOFTWARE FOR A HUMAN VENTRICULAR MYOCYTE MODEL

Cardiovascular diseases (CVDs) are major health problems and the leading cause of death around the world. Cardiac arrhythmias form a significant portion of CVDs which are the electrical production and conduction problems of the heart. Diagnosis and treatment of the cardiac arrhythmias can benefit significantly from a comprehensive understanding of the underlying arrhythmogenic mechanisms. However, the limited availability of experimental data is still a major problem in this field.

Computational modeling is a quite valuable tool in cardiac electrophysiology as it constitutes a backbone for *in silico* simulations based on the existing experimental data. Validated mathematical models can help to uncover the underlying ionic mechanisms of cardiac arrhythmias. Moreover, they can provide benefits to investigate the drug-ion channel interactions and come up with new treatments for cardiac disorders. On the other side, the complexity of the modern cardiac cell models is quite high as they include higher level of physiological details. It can be an error-prone and time-consuming process to code them using conventional programming languages in order to conduct simulations. Thus, an easy-to-use cardiac action potential simulation software and application are designed and developed in this thesis. Furthermore, human ventricular cell models are implemented in order to conduct simulations for heart failure condition and various channel blocker drug effects.

Keywords: Cardiac action potential, computational modeling, simulation software.

ÖZET

İNSAN KALP KARINCIK HÜCRESİ MODELİNE YÖNELİK SİMÜLASYON YAZILIMI

Kardiyovasküler hastalıklar dünya genelinde önemli sağlık problemleridir ve önde gelen ölüm nedenidir. Kalbin elektrik üretimi ve iletimi ile ilgili olan aritmiler kardiyovasküler hastalıkların önemli bir kısmını oluşturmaktadır. Kalp ritim bozukluklarına yol açan nedenlerin kapsamlı bir şekilde anlaşılması aritmilerin tanısı ve tedavisi için oldukça önemlidir. Bununla birlikte deneysel verilerin yeterli düzeyde bulunmaması hala ciddi bir sorun teşkil etmektedir.

Matematiksel modelleme kalp elektrofizyolojisi alanında deneysel verilere dayalı bilgisayarlı simülasyonlar için temel teşkil ettiğinden dolayı oldukça değerli bir araçtır. Geçerliliği kabul edilmiş matematiksel modeller hücresel ve hücre içi düzeyde kardiyak aritmilerin altında yatan iyonik mekanizmaların ortaya çıkarılmasında yardımcı olabilir. Ayrıca bu modeller ilaç - iyon kanalı etkileşimlerini araştırmada ve kalp hastalıkları ile ilgili yeni tedaviler geliştirmede faydalı olabilir. Öte yandan modern kalp hücresi modelleri yüksek oranda fizyolojik detay içerdiklerinden dolayı karmaşıklıkları oldukça fazladır. Simülasyon gerçekleştirmek için bu modelleri konvansiyonel programlama dilleri ile kodlamak hata yapmaya açık ve zaman alıcı bir süreçtir. Dolayısıyla bu tezde kalp aksiyon potansiyeli simülasyonu için kullanımı kolay bir yazılım ve uygulama tasarlanıp geliştirilmiştir. Ayrıca insan kalbi ventriküler hücre modelleri eklenmiş olup bunlar kullanılarak kalp yetmezliği ve çeşitli kanal bloker ilaçların etkileri simüle edilmiştir.

Anahtar Sözcükler: Kalp aksiyon potansiyeli, matematiksel modelleme, simülayon yazılımı.

TABLE OF CONTENTS

LIST OF FIGURES

LIST OF TABLES

LIST OF SYMBOLS

C	Capacitance
cm	Centimeter
d	Distance
ϵ	Dielectric Constant
$IC50$	Half-Maximal Inhibitory Concentration
F	Faraday's Constant
g	Conductance
h	Hill Coefficient
Hz	Hertz
mM	Milli Molar
mS	Milli Siemens
ms	Milli Second
mV	Milli Volt
nM	Nano Molar
nm	Nano Meter
P	Permeability Coefficient
pA	Pico Ampere
pF	Pico Farad
R	Gas Constant
S	Surface Area
T	Absolute Temperature
μA	Micro Ampere
μF	Micro Farad
μM	Micro Molar
z	Valence of the Ion

LIST OF ABBREVIATIONS

4-AP	4-Aminopyridine
AP	Action Potential
APD	Action Potential Duration
API	Application Programming Interface
AVN	Atrioventricular Node
CICR	Calcium Induced Calcium Release
CVD	Cardiovascular Disease
EAD	Early After Depolarization
ECC	Excitation Contraction Coupling
ECF	Extracellular Fluid
ECG	Electrocardiogram
GUI	Graphical User Interface
HF	Heart Failure
HH	Hodgkin-Huxley
ICF	Intracellular Fluid
LA	Local Anesthetic
LMIC	Low- and Middle-Income Country
LR	Luo-Rudy
ODE	Ordinary Differential Equation
OOP	Object Oriented Programming
PB	Priebe and Beuckelmann
redPB	Reduced PB
RyRs	Ryanodine Receptors
SAN	Sinoatrial Node
SCD	Sudden Cardiac Death
SR	Sarcoplasmic Reticulum
TMP	Total Membrane Potential
TTX	Tetrodotoksin

VF	Ventricular Fibrillation
XIP	Exchanger Inhibitory Peptide
XML	Extensible Markup Language

1. INTRODUCTION

In today's industrialized modern world, cardiovascular disease (CVD) has become the primary cause of death in affluent and developing countries. According to the statistics published by the American Heart Association, CVD accounted for nearly one of every three deaths in 2016 in the US [23]. Moreover, 37% of all deaths in the EU, 45% of all deaths in Europe, and 39,7% of all deaths in Turkey are caused by CVD in 2017 [24, 25]. A global point of view indicates an estimation that 31% of all deaths are originated from CVD all over the world [26]. Beyond being a major health problem, CVDs also cause a significant economic burden for governments. The total amount of economic loss due to CVDs in low- and middle-income countries (LMICs) was estimated at about $3,7 trillion between the years 2011 and 2015 [27]. Thus, CVD still remains as a major concern for global health and all nations of the world.

CVDs consist of disorders related to the heart and the blood vessels. Heart diseases form a subgroup of CVDs which affect the heart's function and structure. Structural heart diseases can lead to secondary disorders related to the electrical system of the heart. For example, heart failure (HF) is a disease in which the heart is unable to pump the blood sufficiently to maintain blood circulation throughout the body. Although this is a structural and functional problem, it can also alter the electrical properties of cardiac cells and end up with cardiac electrical system disorders [17].

Besides all its complexness, the heart acts basically as a double-sided pump consists of four chambers. It drives the blood circulation which transports nutrients and oxygen to living cells all over the body as well as removes the harmful metabolic waste from them. The heart consists of about five billion cardiac muscle cells. Contraction of them requires high degree synchronization and rhythmicity for efficient blood pumping action [28]. This is achieved through electrical system of the heart which generates and conducts necessary electrical impulses. Thus, each heartbeat is triggered at a certain pace with coordinated contraction of the cardiac muscle cells [18].

Heart's electrical activity is not a completely isolated process. It can be affected by various factors such as cardiac mechanics, cellular metabolism, coronary blood flow, hormonal factors, and the autonomic nervous system [20]. Electrical impulse production and/or propagation abnormalities in the cardiac electrical system may result in cardiac rhythm disturbances called arrhythmias. Certain types of arrhythmias, especially which are due to the damaged heart structure, can lead to lethal symptoms. For instance, ventricular tachyarrhythmias can induce ventricular fibrillation (VF) which may end up with sudden cardiac death (SCD). VF is the leading cause of more than 250,000 SCD each year in the US [29]. The estimated total incidence of SCD is almost 350,000 annually [30]. Furthermore, morbidity and mortality due to cardiac arrhythmias create an enormous economic impact with an increase in cost per quality-adjusted life year up to US $558,000 [31].

It is broadly accepted that the most lethal arrhythmias are related to the abnormal propagation of wave caused by reentrant excitation sources. On the other side, the underlying mechanisms of initiation and subsequent dynamics of the reentrant sources are mostly unknown due to the fact that possibilities are quite limited to study cardiac arrhythmias invasively in the human heart. Although much study has been carried out on animal hearts differ from mouse to pig, it is a fact that the features of arrhythmias of animal hearts vary significantly from those of the human. For instance, even the size of the pig heart is fairly similar with the human heart, VF frequency is about 10-14 Hz in the pig heart while it is about 5 Hz in the human heart [32]. This is where the computational models of cardiac cells come in and provide significant opportunity to investigate the underlying cellular and subcellular mechanisms of arrhythmias via realistic computer simulations.

Experiments are the primary methods to obtain first-hand data related to the mechanisms of cardiac action potential (AP) generation and propagation. On the other hand, they can be time-consuming and expensive most of the time. Also, careful ethical considerations are required for experiments involving human heart and animal hearts as well. Computational modeling makes it possible to simulate and analyze the complex interplay among several physiological processes leading to contraction of

the heart. Computational models usually contain a mathematical summary of various experimental data collected in years. Experimental data can be gathered about sub-processes of a physiological event, for example, individual depolarizing currents, and an integrative model can be developed based on the collected data which indicates a bottom-up approach [18].

Cardiac cell mathematical models have produced enormous strides since the first model described by Denis Noble in 1962 for Purkinje fiber. Improvements in the experimental techniques led up to higher resolution quantification of cellular physiology. Thus, researchers took the opportunity to develop physiologically more detailed and advanced cardiac cell models based on the plenty of experimental data [1]. The computational cost of the models increased as they became more complex with an increased number of equations, variables, and parameters. A compromise between computability and complexity will be more likely to exist in the future as it does today [33]. Figure 1.1 shows a brief history of cardiac cell models. As can be seen in this figure, the model developed by Hodgkin and Huxley is the common ancestor of a vast majority of cardiac cell models even it has been developed for a nerve cell.

Computer simulations using cardiac cell models provide the researchers with substantial opportunities. First of all, during simulation of a virtual experiment all of the model variables can be observed simultaneously without any intervention required which is not possible in the physical experiments. Also, the user can control the parameters at any time during the simulation and inspect the consequent changes. These advantages of computer simulations make them perfect for testing ideas easily and quickly if they are plausible or not [18]. Thus, models and simulations can be thought of as pre-lab tools which can be used before proceeding physical experiments. Additionally, they can help to improve the experiment procedures and increase the efficiency of experiments.

Cardiac cell models especially which describe detailed subcellular mechanisms generally comprise a large number of equations and state variables. As an example, the Purkinje fiber model developed by Sampson et al. consists of 82 differential

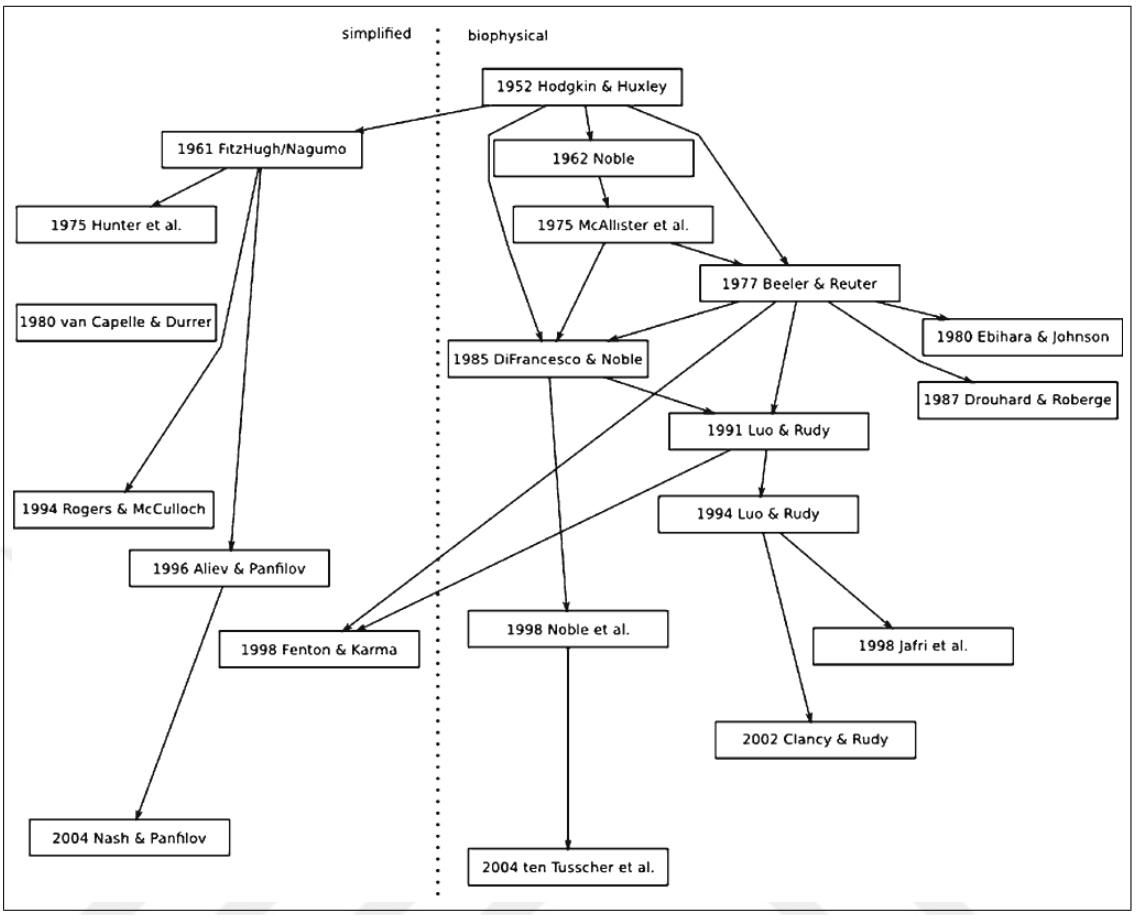

Figure 1.1 Some of the cardiac cell models and ancestors of them [1].

equations [21]. Several tools have been utilized for model implementation and simulation purposes. Researchers usually implement cardiac cell models using numerical or general-purpose programming languages like Java, C, MATLAB, and Fortran. Table 1.1 shows some of the popular tools used in the model implementation and the number of times they are mentioned in papers.

Obviously, it is an error-prone and time-consuming process to implement the complex cardiac cell models with a large number of equations using any of the programming languages. Hence, it can be tedious to obtain the same results claimed in the papers published by the model developers. Sometimes researchers share the source code of their model implementation in various platforms. However, this time the other researchers who would like to modify or use the source code should be familiar with the programming language in which the code is written. A number of easy-to-read

modeling languages have been developed in order to address this issue. CellML is a famous one among the modeling languages in the life sciences field. The main goal of CellML is to increase accessibility and reusability of the mathematical models related to the biochemical and electrophysiological processes. However, although it is human-readable and machine-readable XML based language, it is not easy to write by hand and it is not easy to read as well [18].

Table 1.1
Popular tools used in model implementation [18].

Tool	Mentions
Matlab	22
C	17
C++	12
Fortran	10
COR	3
Java	2
Octave	1
Chaste	1
CMISS	1
Berkely Madonna	1
Unknown	6

To sum up, cardiac cell models have significant importance for cellular cardiac electrophysiology studies. They can help to uncover the underlying mechanisms of electrical activity related to cardiac disorders and drug-ion channel interactions. Moreover, they can be utilized for educational and scientific research purposes. On the other side, most of the current models share the same problem of limited accessibility and flexibility. Accessibility limitations indicate obstacles to obtain the source code and lack of adequate user-friendly interface. An accessible model should be effortless to use for students as a learning tool and for researchers as a development tool. Moreover, it should not necessitate programming skills in order to modify the model parameters and run the simulation [34]. The main purpose of this thesis is to develop such kind of simulation program and MATLAB based application in order to fill this gap and free the valuable resources for physiological studies.

2. BACKGROUND: CARDIAC ELECTROPHYSIOLOGY

This section gives a basic outline of the heart anatomy and the cardiac electrophysiology aiming to set a ground for subsequent chapters.

2.1 Anatomy and Function of the Heart

The human heart is a muscular organ which pumps the blood to the systemic and pulmonary circulations consistently and makes a crucial contribution for vitality. It starts to beat independently when embryo enters the fourth week yet more before the innervation formed and continues to beat approximately 100,000 times per day until death [35]. The heart receives deoxygenated blood coming from various tissues throughout the human body and pumps it into the lungs for oxygenation. Consequently, the oxygenated blood flows back to the heart and this time it pumps the oxygenated blood back to the tissues all over the body. Furthermore, another function of the heart is to produce cardiac hormones to help maintain blood pressure.

The heart is positioned obliquely across the middle mediastinum of the thoracic cavity and located in a serous membrane sac named pericardium which has a lubricating fluid in it [36]. Heart's outer surface is lubricated by the pericardial fluid to make it freely move in the pericardial cavity during contraction and relaxation phases. Three layers, parietal, visceral, and fibrous, form the structure of the pericardium. The visceral layer, named epicardium, basically made up of connective tissue. It covers the heart's outermost surface and base of the large vessels. Due to various pathological circumstances, the pericardial cavity can collect fluids or blood exceedingly which ends up with dropsy of the pericardium, also known as cardiac tamponade [4].

The myocardium is a contractile muscular tissue located beneath the epicardium and constitutes the walls of the heart chambers. Cardiac muscle fibers construct the myocardium in a dendritic structure form and they have a bunch of characteristic

features in comparison to the other muscle fibers in the body. First of all, each of the cardiac muscle cells includes single nuclei located in the center of the cell. Moreover, cardiac muscle cells connect to each other through intercalated discs as depicted in Figure 2.1 which ensure the integrity of the myocardium and provide transmission paths for high-speed conduction of electrical impulses among the cells. Calcium (Ca^{2+}) ion influx triggers contraction of the myocardium. Also, the cardiac muscle cells possess intrinsic contraction capability which makes the heart able to maintain its own beat independently [35]. The myocardium receives blood supply from the coronary arteries originating from the aortic root. If these arteries get occluded due to various reasons, thrombosis, for instance, this situation can lead ischemia which indicates a deprivation of the oxygen in the myocardium. Long-standing ischemia eventually ends up with necrosis of the myocardial tissue also known as myocardial infarction.

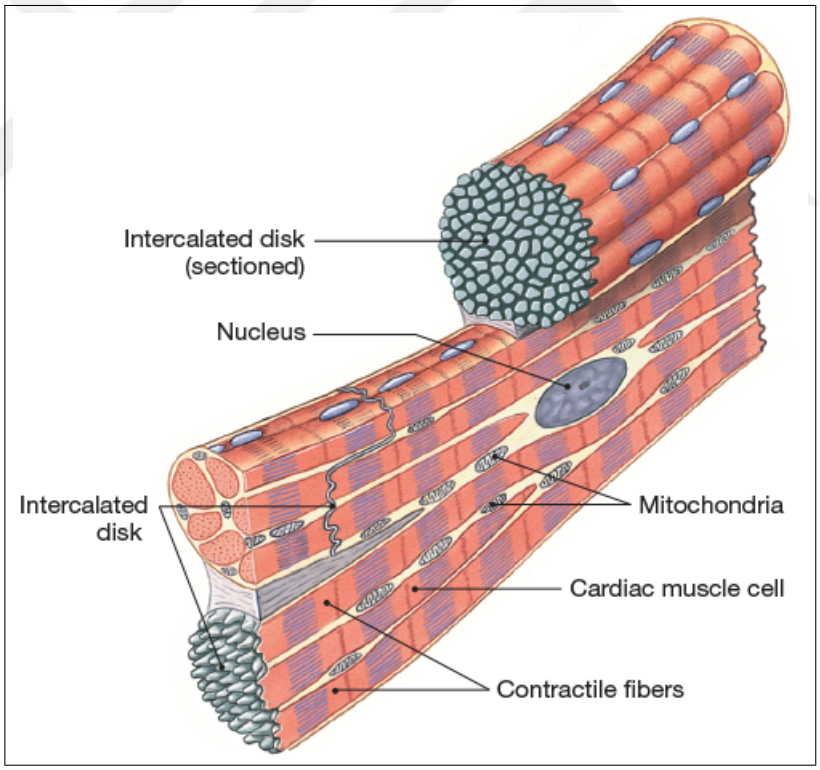

Figure 2.1 Structure of the cardiac muscle tissue. Each of the cardiac muscle cells contacts the others through intercalated disks [2].

The innermost layer of the heart, named endocardium, coats the interior surface of the heart chambers and surface of the heart valves. The endocardium is made up of squamous epithelium cells and it forms a thin sheet named endothelium. Smoothness

is the most significant feature of the endocardium and thanks to this feature, it avoids abnormal blood clot formations [35].

The heart contains four chambers, two atria, and two ventricles as shown in Figure 2.2. Right and left atrium constitute the upper section of the heart and these chambers are internally split up through a common myocardial tissue named interatrial septum. The location of the atria is considered as the base of the heart where all of the great vessels are connected to. Right and left ventricles are the lower side chambers of the heart and they are internally divided by the interventricular septum. Ventricles have thicker walls in comparison with atria as they need more muscular force to pump the blood either to the body and to the lungs. A fibrous tissue named cardiac skeleton separates the ventricles from the atria in order to provide electrical isolation between the ventricular myocardium and the atrial myocardium [4].

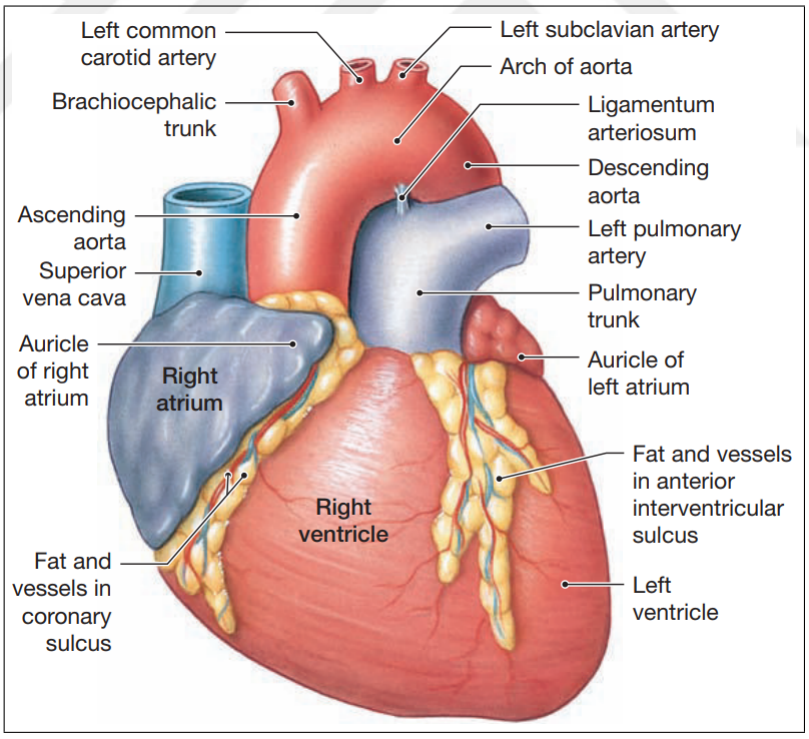

Figure 2.2 Anterior section of the human heart with major anatomical structures [2].

Two great veins, inferior vena cava, and superior vena cava are connected to the right atrium of the heart and carry the oxygen-free blood from lower and upper parts of the body, respectively. Tricuspid valve can be thought of as a one-way gate connecting

the right atrium to the right ventricle. It consists of three cusps which are made up of connective tissue and each of them has a connection to the right ventricle through the papillary muscles. Thus, ventricle contraction forces the cusps upwards and makes the tricuspid valve closed to avoid blood flowing back from the right ventricle to the right atrium. Oxygen-free blood in the right ventricle is pumped to the lungs flowing through the pulmonary semilunar valve and the pulmonary artery. The pulmonary valve resides at the junction of the right ventricle and the pulmonary artery. It maintains a one-way flow of the blood to the lungs and avoids backflow to the right ventricle. The oxygen-free blood gets oxygenated in the lungs and flows through the pulmonary veins into the left atrium. The left ventricle receives the oxygen-rich blood from the left atrium. Mitral valve resides between the left atrium and the left ventricle. It avoids blood flowing back to the left atrium when the ventricular contraction occurs. Oxygenated blood in the left ventricle joins to the systemic circulation passing through aorta which is known as the largest artery in diameter in the human body. Aortic semilunar valve resides at the junction of the left ventricle and closes when the left ventricle gets relaxed. The left ventricle has a thicker wall in comparison with the right ventricle in order to provide a forceful pumping action [37].

2.2 The Cardiac Electrical System

The heart has five main physiological properties which are conductivity, automaticity, excitability, contractility, and rhythmicity. Coordinated and rhythmic contractions are crucial in order to maintain an efficient pumping action of the heart. For this purpose about 10^{10} myocytes should contract in a coordinated manner [38]. The cardiac electrical system initiates and conducts required electrical impulses in order to maintain rhythmic and automatic contractions of the heart. Five specialized cell networks constitute the cardiac electrical system. They are named as sinoatrial node (SAN), atrioventricular node (AVN), bundle of His, bundle branches, and Purkinje fibers as illustrated in Figure 2.3.

The SAN is the natural cardiac pacemaker which locates at the lateral junction of the superior vena cava orifice and the right atrium. It is discovered by Keith and Flack and published in 1907 [39]. The SAN consists of special cardiac muscle cells. They have higher permeability of sodium (Na^+) ions in comparison with other cardiac muscle cells. Hence, the cells of SAN depolarize faster and trigger each heartbeat. Intrinsic impulse generation frequency of the SAN is about 70/min which is higher than the other parts of the cardiac electrical system. Therefore, the SAN is dominant in the impulse generation mechanism while the other parts remain silent [40].

Additionally, Bachmann's bundle conducts electrical impulses from the right atrium to the left atrium through interatrial septum. Thus, both of the atria contracts together when the SAN generates each electrical impulse [39].

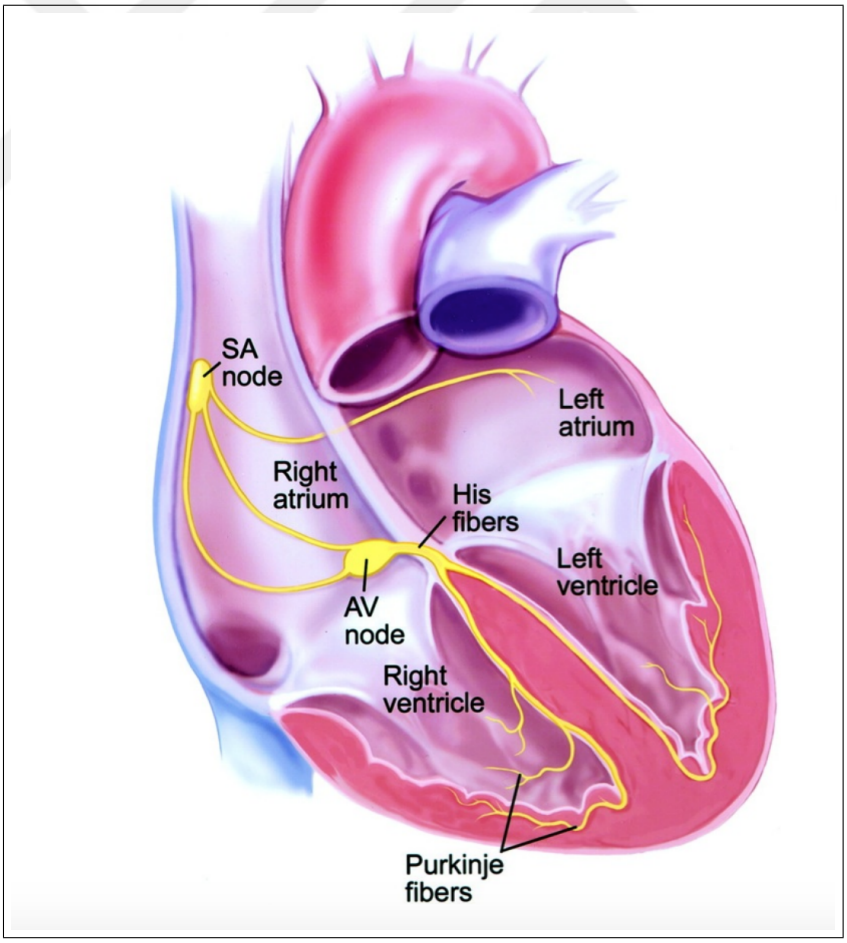

Figure 2.3 The cardiac electrical system with conduction pathways and major pacemaker nodes [3].

Electrical impulses spread from the SAN through internodal pathways to the AVN which is located within the Koch triangle in the right atrium. *Crista terminalis* and interatrial septum are electrical inputs of the AVN for the impulses coming from the atria [41]. Atrial systole occurs when the electrical impulses arrive at the AVN. A fibro-adipose tissue insulates the ventricular myocardium from the atrial myocardium at the atrioventricular junction. The penetrating atrioventricular bundle, also named as the His bundle is the only pathway of electrical continuity between ventricular and atrial myocardium [42]. The AVN conducts electrical impulses with an approximately 0,1-second delay to ensure that the atria get drained completely before contraction of the ventricles. The conduction delay also provides adequate time for the atria to overfill the ventricles prior to the ventricular contraction. This helps to keep the output of the heart at the highest level in each contraction. Moreover, in case of rapid atrial depolarization, for instance, atrial flutter or atrial fibrillation, the AVN avoids fast conduction of the impulses to the ventricles. The intrinsic impulse frequency of the AVN is about 50-60/min which is lower than the sinus rhythm [40].

The ventricular conduction network consists of His bundle, right-left bundle branches (Tawara branches), and the Purkinje fibers. After the AVN, the electrical impulses move through the His bundle and Tawara branches, then spread all over the ventricles through the Purkinje fiber network which ends up with the ventricular systole.

2.3 The Cardiac Action Potential

The cardiac AP stands for an electrical stimulus which is generated by orchestrated ion fluxes through the ion channels embedded in the excitable cardiac cell membrane. All of the cardiac cells possess the ability to conduct electrical impulses. On the other side, a population of them is specialized to generate APs in an inherent and rhythmical manner. About 1% of the cardiac cells in other words cardiomyocytes turn into autorhythmic and self-excitable form during the embryonic development [7]. The electrical system of the heart is made up of such kind of cardiomyocytes. The

AP fired by the SAN spreads through the cardiac conduction pathway and excites the contractile ventricular and atrial muscle fibers.

The electrochemical gradient for several ions across the cell membrane determines the resting membrane potential. It is maintained by the activity of ion pumps and selective channels of the cell membrane. Potassium (K^+) ion is the major factor in terms of determination of the resting membrane potential in cardiomyocytes. Normally K^+ ion concentration is higher in the cytoplasm than the extracellular region as shown in Figure 2.4. Moreover, the permeability of the cell membrane is higher for K^+ ions than the other compounds and ions exist in the cytoplasm. Therefore, K^+ ions have a tendency to leave the cell however an electrical gradient counters this tendency which describes the Donnan equilibrium [12].

The ion concentration difference across the cell membrane ends up with an electrical potential, also referred to as the equilibrium potential which is formulated by the Nernst equation shown by Eq. 2.1.

$$E_{ion} = \frac{RT}{zF} \times ln\frac{[Outside]}{[Inside]} \tag{2.1}$$

where T is the absolute temperature, R is the gas constant, F is the Faraday's constant, z represents the valence of the ion, $[Outside]$ is the extracellular ion concentration, and $[Inside]$ is the intracellular ion concentration [12].

The membrane potential of the cardiomyocytes is roughly $-90\ mV$ at the resting state and K^+ ions have a major contribution on it [4]. Goldman-Hodgkin-Katz equation referred to as Eq. 2.2 provides a more precise description of the membrane potential by taking into account the other ions [43].

$$E_m = \frac{RT}{zF} \times ln(P_K \frac{[K_o]}{[K_i]} + P_{Na} \frac{[Na_o]}{[Na_i]} + P_{Cl} \frac{[Cl_i]}{[Cl_o]}) \tag{2.2}$$

where P_K, P_{Na} and P_{Cl} are the permeability coefficients; $[K_o]$, $[Na_o]$, and $[Cl_o]$ are the extracellular ion concentrations; $[K_i]$, $[Na_i]$, and $[Cl_i]$ are the intracellular ion concentrations for K^+, Na^+, and Cl^- ions, respectively. As shown in this equation, the concentration gradient across the cell membrane and membrane's permeability for a specific ion determines the contribution of that ion to the membrane potential of the cell.

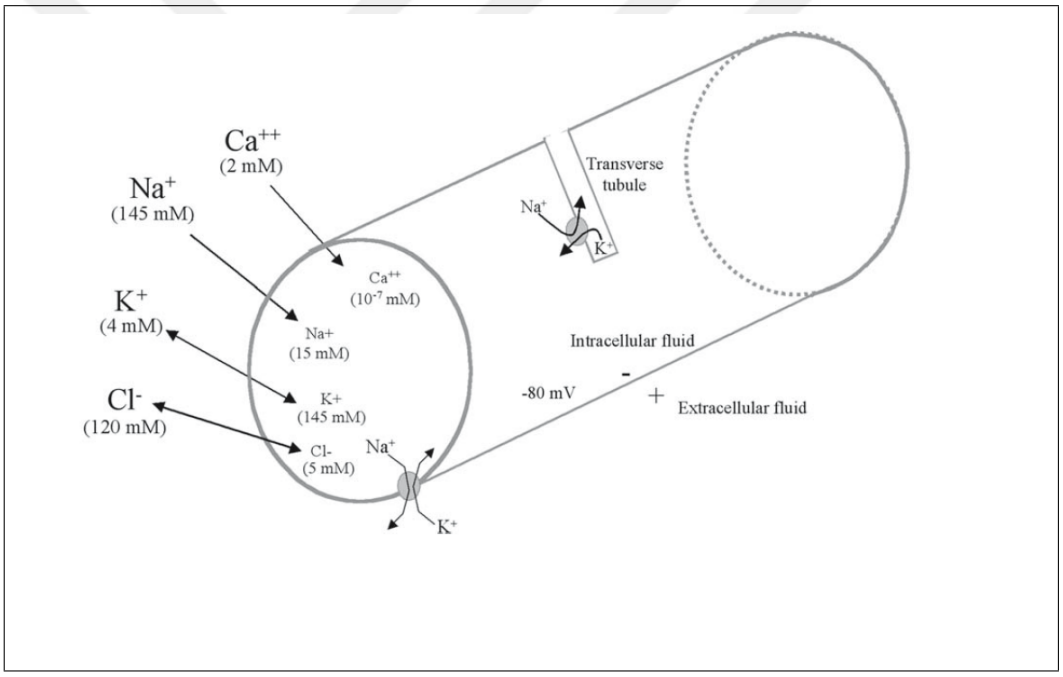

Figure 2.4 Characteristic ion concentrations for the cardiac cell [4].

At the resting state, cardiomyocytes have a negative electrical gradient in reference to the extracellular fluid. It describes electronegativity of the cytosol and sign of the membrane potential at resting state. The ion permeability of the cell membrane changes in consequence of an electrical stimulus above a certain threshold. The transient alterations of the cellular ion permeability generate cardiac APs. The phases and ion flow characteristics with regard to each phase are shown in Figure 2.5.

When a super-threshold electrical stimulus reaches to the cardiomyocyte which is at the resting state (Phase 4) with an approximately $-90\ mV$ membrane potential, the voltage-gated fast Na^+ channels open instantly. Consequently, Na^+ ions flow into the cell rapidly due to two reasons. Firstly, the intracellular environment is electrically more negative in comparison with the extracellular environment. Secondly, the Na^+ concentration is higher in the extracellular environment [12]. Hence, the decrease in the electrochemical gradient ends up with rapid depolarization (Phase 0) of the cell within a few milliseconds.

After the fast Na^+ channels get inactivated, initial repolarisation phase (Phase 1) begins with opening of the transient outward current (I_{to}) channels and the K^+ ions flow outside of the cell. Ventricular wall of the heart has heterogeneous I_{to} channel expression. Hence, prominence of Phase 1 is higher in subepicardial layers as compared to subendocardial tissue.

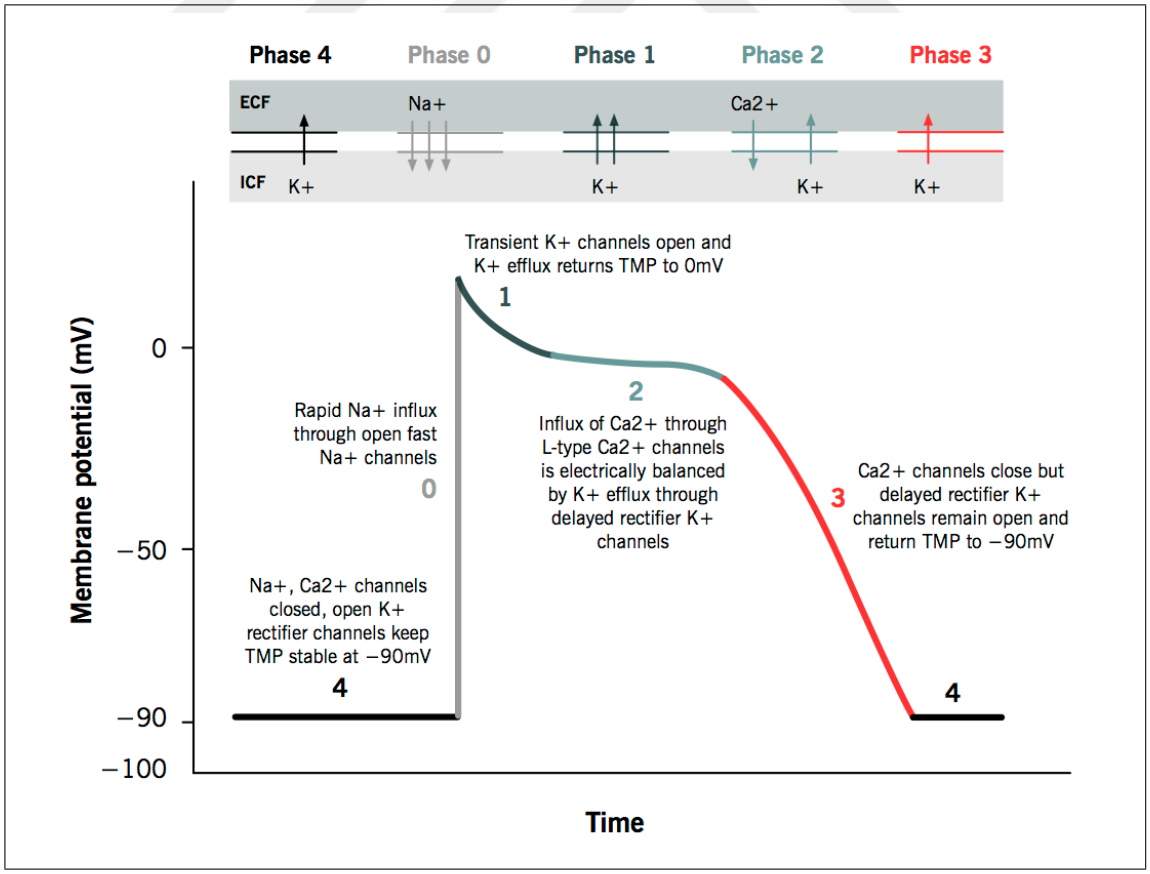

Figure 2.5 Cardiac AP phases and the ion flow characteristics [5].

The voltage-gated L-type slow Ca^{2+} channels open in order to slow down the repolarization state. The extracellular environment has a higher Ca^{2+} concentration, so the Ca^{2+} ions flow into the cell due to the concentration gradient. This ion flow triggers sarcoplasmic reticulum (SR) to release Ca^{2+} ions into the cytoplasm. Eventually, the calcium concentration increases in the intracellular environment and Ca^{2+} ions bind to the troponin C which ends up with contraction of the ventricular contractile fiber. This second phase (Phase 2) of the cardiac AP is named as the plateau phase. In the plateau phase, some of the depolarization-activated voltage-gated K^+ ion channels remain open and allow the K^+ ions flow to the extracellular environment in order to promote repolarization. Delayed rectifier current (I_K) stands for this type of outward current. On the other side, Ca^{2+} influx balances the K^+ ion efflux and depolarization state is maintained in the course of the plateau phase which takes about 0,25 second. Skeletal muscle and neuron lack the plateau phase contrary to the cardiac muscle [7].

In the rapid repolarization phase (Phase 3), the L-type Ca^{2+} channels close and leave the K^+ ion flow alone. K^+ efflux continues until the resting value of the membrane potential is reached. By the end of this phase, $Na^+ - K^+$ pump moves Na^+ ions out of the cell and K^+ ions into the cell simultaneously. Also, the remaining Ca^{2+} ions in the cytosol are moved out by the $Na^+ - Ca^{2+}$ exchanger [44].

The AP characteristics change in different parts of the heart as illustrated in Figure 2.6. SAN and AVN cells have short lasting APs. They are lack of initial repolarization and plateau phases. A slow rise from the resting membrane potential activates the T-type Ca^{2+} channels when it reaches the threshold and depolarization occurs with Ca^{2+} influx. Voltage-gated K^+ channels trigger the repolarization phase and leak channels help to keep resting membrane potential unstable for the next activation of the T-type Ca^{2+} channels. On the other side, ventricular and atrial myocytes also the Purkinje fibers are fast-response cells which possess a fast transition phase from resting potential to depolarization because of activation of the voltage-gated Na^+ channels. This rapid transition can be observed as a notch in the AP shape. L-type Ca^{2+} channels and voltage-gated K^+ channels maintain a balance between Ca^{2+} influx and K^+ efflux in the plateau phase. Action potential duration (APD) is about 150 ms for the

nodal cells, 250 ms for the ventricle myocytes, and 300 ms for the Purkinje fibers [4].

The cumulative sum of the APs emerge from different regions of the heart can be sensed on the surface of chest skin through appropriate electrodes and device, named as the electrocardiogram (ECG). The ECG signal provides significant information about cardiac electrical activity and performance of the contractile components of the heart. For instance, an abnormal pattern can be seen in the ECG signal when the heart has a conduction impairment due to various reasons. A healthy ECG signal is illustrated in Figure 2.6. In this figure, the P wave indicates the atrial depolarization. Contraction of the atria starts about 25 ms later following the P wave. Ventricular depolarization can be noted as QRS complex where the electrical signal is comparatively powerful due to the thicker muscular wall of the ventricles than the atria. The ventricular contraction occurs shortly after the R wave peak of the QRS complex. Finally, ventricular repolarization is accompanied by the T wave. Atrial repolarization occurs during the ventricular depolarization [7]. The electrical event of the atrial repolarization is masked by the QRS complex. Therefore, it can not be observed on the ECG signal.

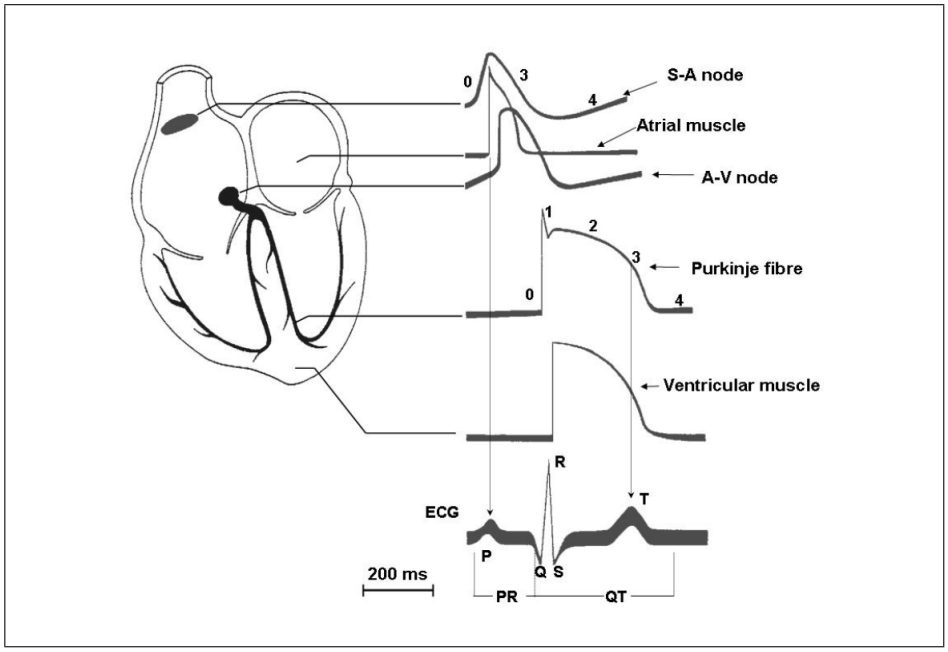

Figure 2.6 AP shapes from different regions of the heart and the ECG formation [6].

2.4 Cardiac Ion Channels and Membrane Currents

The orchestrated flow of various ions through cardiac cell membranes produces required electrical potentials in order to excite the heart and trigger the pumping action. The cardiac cell membrane has a lipid bilayer structure and does not let the charged ions pass across the membrane directly due to the hydrophobic phospholipid layers. Hence, some of the membrane proteins form aqueous hydrophilic channels across the cell membrane so as to allow the ion transitions. The ion channels possess selective permeable feature and they can be categorized based on their gating mechanisms, for example, ligand-gated ion channels and voltage-gated ion channels. The opening and closing of the voltage-gated ion channels are dependent on the cell membrane's electrical potential and elapsed time after the membrane potential alteration.

Electrical stimulus above a certain threshold activates the voltage-gated ion channels of the cardiac myocyte and ends up with the inward flow of positively charged ions to the cytoplasm. Thenceforth, the electronegativity decrease in the cytoplasm causes the cell membrane to depolarize. The cell membrane returns back to its resting electrical potential when outward currents restore the electronegativity of the cytoplasm which is called repolarization. K^+ efflux is the major outward current which generates repolarizing currents in the heart. The inward flow of anions such as chloride can also support the repolarization. On the other side, the major depolarizing inward currents are generated by the positively charged Ca^{2+} and Na^+ ions as shown in Table 2.1.

Table 2.1
Properties of major ion fluxes across the cardiac cell membrane [19].

	Charge	Flow Direction	Generated Current	Effect
Calcium	Positive	Inward	Inward	Depolarization
Sodium	Positive	Inward	Inward	Depolarization
Potassium	Positive	Outward	Outward	Repolarization
Chloride	Negative	Inward	Outward	Repolarization

2.4.1 Calcium Channels

Calcium channels have crucial importance on the excitability of the heart and mechanical contraction properties of the cardiac muscle cells. Several types of calcium channels exist in mammalian excitable cells. The most important types for the heart are the T-type (transient and tiny) and L-type (long-lasting and low threshold) calcium channels [12].

L-type calcium channels allow Ca^{2+} entry into the cell in order to maintain the AP plateau which is the dominant phase in the cells of ventricles, atria, and Purkinje fibers [6]. On the other side, in the rapid depolarization phase, L-type calcium channels open right after the activation of Na^{+} channels and make a little contribution to the total inward current of positively charged ions. Hence, it is named as slow or secondary inward current [12].

Cardiac contractility is maintained through alterations of the intracellular calcium ion concentration. Approximately 20% of required Ca^{2+} for cellular contraction comes from the extracellular environment through the L-type calcium channels throughout the AP plateau phase [2]. Yet, the large portion of Ca^{2+} is obtained from calcium storage of the SR. In the plateau phase, extracellular calcium ions flow into the cytosol passing through the L-type calcium channels. The small amount of Ca^{2+} influx triggers the release of reserved Ca^{2+} from the SR into the cytoplasm through Ryanodine receptors (RyRs). This action is named as calcium-induced calcium release (CICR) [45]. Consequently, calcium ions in the cytoplasm bind to the troponin C in order to enable actin-myosin cross-linking and contraction of the cell [46]. In some kinds of triggered arrhythmias such as early after depolarization (EAD), the underlying inward current can be supported by the L-type calcium channels. Therefore, they have a substantial role in the occurrence of arrhythmogenesis. Furthermore, in the reentrant circuits, the slow conduction can be supported by the calcium channels [1].

T-type calcium channels generate a small amount of inward current during depolarization in comparison with sodium channels which provide the large portion of the

inward depolarizing current. Thus, the role of T-type calcium channels is not crucial for the depolarization phase of the AP [12]. T-type calcium channels are re-expressed in ventricular and atrial cells under a variety of pathological cases, for instance, HF and cardiac hypertrophy. Despite the fact that they make less contribution to the CICR mechanism than the L-type calcium channels, under several pathological circumstances T-type calcium channels are involved in the disruption of excitation-contraction coupling (ECC) and abnormal cardiac electrical activity [47].

2.4.2 Sodium Channels

The voltage-gated sodium channels give rise to APs in a variety of excitable cells such as cardiac myocytes and neurocytes. They open rapidly within about 3 ms and generate fast inward current to depolarize the working cells of ventricles and atria, as well as the conducting cells of Purkinje fibers and His bundle [6]. Additionally, sodium channels can contribute to the plateau phase of the AP through a very small amount of long-lasting inward current which is named as late sodium current [12].

Mutations of sodium channels can lead to fatal arrhythmias. For instance, a mutation with an effect of increased late sodium currents will cause delayed repolarizations and eventually end up with long QT syndrome, LQT3. Conversely, the mutations which decrease the opening rate of the sodium channels give rise to electrocardiographic abnormalities named as Brugada syndrome [12]. These syndromes can cause VF and end up with SCD. Furthermore, sodium channels play a central role in the propagation of the APs and reduce of the sodium current will disrupt the propagation which can induce arrhythmias. The balance between repolarizing and depolarizing currents throughout the plateau phase of the AP can be disturbed through persistent sodium current as a consequence of sodium channel mutation. This can induce EAD by extending the APD [1]. The sodium channels can be blocked through local anesthetic (LA)/class I antiarrhythmic agents to suppress the excitability of cardiac myocytes. Thus, the LA compounds are generally utilized for the treatment of electrical propagation and excitability related disorders such as cardiac arrhythmias even their success

rate is limited [48].

2.4.3 Potassium Channels

The voltage-gated potassium channels are primarily responsible for cardiac repolarization via generating the large portion of outward currents. In comparison with the other voltage-gated channels, potassium channels have a higher diversity as more than 12 subtypes of them contribute to the electrophysiology of the cardiac cells [1]. Some types of potassium currents and functions of them are shown in Table 2.2. Mutual interaction between the electrical potential of the cell membrane and potassium channel's opening/closing is usually explained as rectification of the transmembrane current flow. The unrectified current is a result of constant membrane resistance over a series of various membrane potentials [19].

The inward rectifying potassium current, I_{K1}, maintains and stabilizes the resting membrane potential. When the membrane potential falls below the Nernst potential for potassium, inward rectifying potassium channels promote the influx of positively charged ions to restore the resting value of the membrane potential. Around the Nernst potential, these channels have high conductance which contributes to maintaining a stable membrane potential during diastole [1]. On the other side, inward rectifying channels close upon depolarization which ends up the reduction of repolarizing current. This helps to prolong and control the plateau phase of cardiac AP. Acidosis and increased intracellular calcium concentration can inhibit the I_{K1} current [12].

A group of potassium channels opens and generates the outward transient current (I_{to}) right after the upstroke of AP. This is produced by the fast inward current of the sodium ions [19]. The early repolarization phase is maintained via the repolarizing current I_{to}. Moreover, during the plateau phase, I_{to} can support the balance between outward and inward ionic currents. The APD and refractoriness are modulated by the I_{to}. In fact, this transient current is dominant in the atria which can be responsible for the shorter APD in the atrium [1].

In the terminating phase of the AP (Phase 3), the delayed rectifier currents play the central role by contributing to repolarization of the cardiomyocytes. The major constituents of the delayed rectifier currents are named as the rapid delayed rectifier current (I_{Kr}) and the slow delayed rectifier current (I_{Ks}). I_{Kr} starts to flow right after the depolarization and gets the peak value by the end of the plateau phase [12]. On the other side, I_{Ks} has a delayed and slow activation property as its flow rises gradually during the plateau phase of the AP. Abnormalities in I_{Kr} channels can cause LQT2 or short QT syndrome and both of them may end up with lethal arrhythmias through disrupting the repolarization mechanism [1].

Table 2.2
Major cardiac potassium currents [19].

Type	Function
Inward (anomalous) rectifying	Maintains the resting potential, prolongs the plateau, and closes with depolarization
Outward (delayed) rectifying	Initiates repolarization, opens by the end of the plateau phase
Transient outward	Contributes to early repolarization, opens immediately and briefly after depolarization
Calcium activated	Activated as a result of high cytoplasmic calcium concentrations, speeds up repolarization in the heart with calcium-overload
Sodium activated	Activated as a result of high cytoplasmic sodium concentrations, may support repolarization in the heart with sodium-overload
ATP-sensitive	Suppressed by ATP under normal conditions, opens in the heart with energy-starvation
Acetylcholine-activated	Activated through vagal stimulation and adenosine, hyperpolarizes resting cardiac cells, slows SAN cells, shortens atrial AP
Arachidonic acid-activated	Activated by arachidonic acid and the other fatty acids, particularly at the acid pH

3. MODELING CONCEPT OF EXCITABLE CELLS

Excitability of certain type of cells is essential for the vitality of human being as well as the other living beings. Excitable cells such as β-cells in the pancreas, neurons in the brain, and cardiac cells in the heart produce and conduct electrical impulses mainly owing to dynamic ionic variations between intracellular and extracellular mediums. The electrical activity ends up with various crucial physiological effects in various tissues. For instance, as a result of the electrical activity, β-cells secrete the insulin hormone to regulate the glucose level in the blood and pacemaker cells maintain a rhythmic contraction of the heart for pumping the blood adequately [35]. Hence, comprehending the underlying mechanisms of cellular excitability is important to get a holistic view of the physiological processes and related disorders.

Mathematical models feature in all fields of science, from quantum physics to quantitative biology. Experiments and observations provide significant information about the inherent mechanisms of nature and help us develop theories in regard to the behavior of nature. Models are developed based on a number of hypotheses and theories in order to predict observation and experiment results. The predictions can be compared with actual experimental results to validate the model and the underlying hypotheses and theories [49]. A valid and accurate model is a quite valuable tool to conduct computer simulations under a variety of virtual conditions and trying different parameters in an easy way. In the context of excitable cells, it would be a quite efficient method to conduct voltage clamp simulations on the computer in order to investigate the underlying ionic mechanisms of cellular AP generation and conduction. Moreover, mathematical models and simulations can be used to reduce required laboratory experiments and costs in the pharmaceutical industry. For instance, the average cost of a novel drug development process is about US$ 900 million and R&D costs are prominent in this process [50]. The costs and time to market could be reduced by using validated models and computer simulations.

Mathematical modeling studies of the heart go back to 1928 when van der Pol and van der Mark claimed a numerical expression of the heartbeat in the form of relaxation oscillations [51]. On the other side, Bernstein proposed a theory about excitation and conduction related to excitable cells in 1902 and it was widely accepted until the late 1930s. According to this theory, the potassium concentration in the cell was about 50 times higher than the extracellular environment and the cell membrane was selectively permeable to the potassium ions. Excitation was explained as an increase in ion permeability of the cell membrane which ends up with an increase of the measured potential from 50-100 mV negative to nearly zero. So the permeability of the membrane changes based on the potassium ion concentration in the cytosol. Cole and Curtis conducted a series of experiments with excitable cells of *Nitella* and giant axons of squid in 1938. The results of the experiments were parallel with Bernstein's theory [52]. After World War II, more advanced equipment became accessible to conduct detailed experiments and intracellular recordings. In 1951, Hodgkin and Huxley performed voltage clamp experiments on a giant axon of squid to investigate the AP generation and propagation mechanisms. Consequently, they obtained plenty of quantitative data and based on the experimental results they came up with a set of ordinary differential equations (ODE) to make a mathematical description of the membrane currents. They also proposed an electrical equivalent of the cell membrane. In 1952, Hodgkin and Huxley's work was published as a series of paper and due to this remarkable scientific achievement, they were honored with Nobel Prize in Physiology [53]. Thenceforth, their modeling approach of membrane currents and AP has been widely utilized in excitable cell studies and computer simulations, even today.

3.1 Electrical Equivalent of the Excitable Cell Membrane

The cytoplasm of an excitable cell is isolated from the external environment through a semi-permeable flexible membrane which is made up of cholesterol, phospholipids, and proteins. The phospholipids compose 75% of the membrane lipids and they are arranged as a back-to-back double layer which is named as lipid bilayer structure as depicted in Figure 3.1. A small amount of (around 20%) cholesterol reduces the

fluidity of the membrane in order to increase the stability of it [7]. The lipid bilayer structure has polar and nonpolar regions. The polar region consists of phosphate containing a hydrophilic head group of phospholipids. Fatty acid containing hydrocarbon tail group forms the nonpolar region of the bilayer structure which has a hydrophobic characteristic. Lipid-soluble compounds can easily enter or leave the cytoplasm by diffusion through the plasma membrane due to the phospholipids in the membrane structure [35]. Some of the integral membrane proteins compose ion channels and pores to let charged ion flow between intracellular and extracellular environments. Most of the ion channels selectively allow passage of just one kind of ion. Furthermore, integral proteins form transporters which actively carry the polar substance to inside or outside of the cell through the membrane [7].

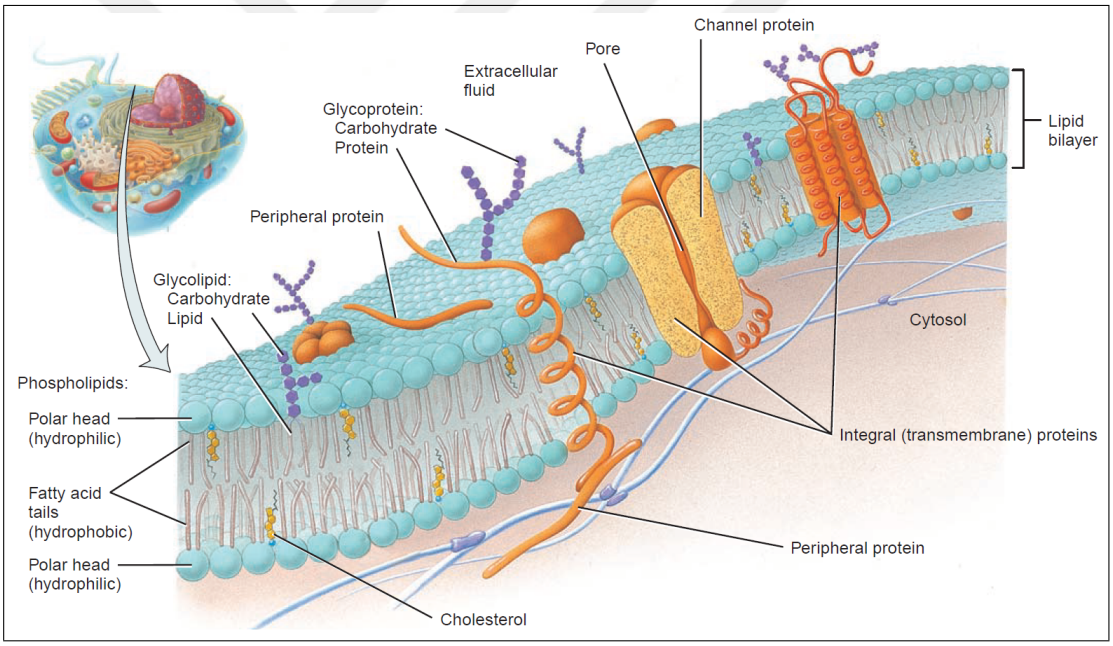

Figure 3.1 Structure of the cell membrane [7].

Uncharged compounds can dissolve in the lipid bilayer structure and diffuse through it. On the other side, charged compounds and ions can only flow through channels and exchangers. The semi-permeability and thinness of the lipid bilayer structure end up with separated charges at a short distance about 20-30 nm and promotes the electrostatic interaction between them. Thus, the cell membrane behaves as a capacitor with high dielectric constant [20]. The related structure and electrical equivalent of the cell membrane are depicted in Figure 3.2.

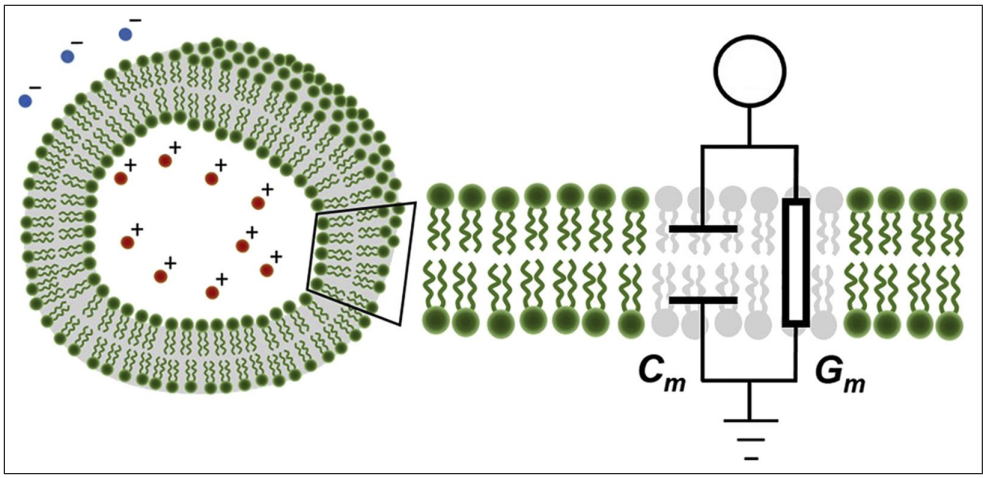

Figure 3.2 Lipid bilayer structure of the cell membrane and the equivalent circuit consists of capacity (C_m) due to amphipathic phospholipid layers and resistance ($1/G_m$) due to the ion channels [8].

The capacity of the membrane C_m is described by the equation referred to as Eq. 3.1.

$$C_m = \frac{\epsilon \times S}{d} \tag{3.1}$$

where S refers to the surface area of the cell, d is the distance between intracellular and extracellular electrolytic environments of the cell, ϵ is the dielectric constant of the phospholipid bilayer membrane structure.

The total charge Q_m stored by the membrane can be calculated by

$$Q_m = C_m \times E_m \tag{3.2}$$

where C_m is the capacity of the membrane in F and E_m is the membrane potential in V.

Invaginations of the membrane such as *caveolae* and T-tubules increase the proportion of the membrane surface area to the volume of the cell. Capacity per unit membrane surface area describes the specific capacitance and it is quite the same among the biological cell membranes which is about 1 $\mu F/cm^2$ [20].

Two types of currents exist on the cell membrane. One of them is the ionic currents. The inward ionic current stands for the positive ion movement from outside to the inside of the cell. Inward ionic currents cause depolarization of the cell membrane by decreasing the resting state electronegativity of the cytoplasm. Moreover, efflux of negative ions causes a similar effect with inward ionic currents on the membrane's electric potential. The positive ion flow from inside to the outside of the cell creates outward ionic currents which increase electronegativity of the cytoplasm. The influx of anions causes the same effect with the outward ionic currents. After the depolarization state, outward ionic currents induce repolarization for recovering the resting state electronegativity of the cell. On the other side, outward ionic currents cause hyperpolarization if the cell is already in the resting state [12].

Capacitive current is the other type of membrane currents which is produced by moving of electrons relative to the membrane's surface. When a cathode is placed near the cell's outer surface in the resting phase, positive charges on the extracellular surface will move towards the cathode and the total positive charge will decrease on the surface. Consequently, the negative charges will move away from the intracellular surface which will end up with the discharge of the membrane capacitance and depolarization of the cell. Capacitive currents are the initiator of the APs and triggered by a depolarization wave approaching to the resting myocyte [12].

The resistance of the cell membrane R_m can be represented by Ohm's law stated below,

$$R_m = \frac{E_m}{I_m} \tag{3.3}$$

where R_m is the membrane resistance, E_m is the electrical potential of the membrane, and I_m stands for the total membrane current flow.

The conductance of a myocyte G_m defines the unidirectional charge flow through the membrane and it is specified as the inverse of the membrane resistance. On the other side, permeability P_m indicates the bidirectional flow of charges or compounds through the membrane. The flux of a compound can be calculated by,

$$Flux = -P \times \Delta c \tag{3.4}$$

where P is the permeability coefficient of the compound and Δc is the concentration difference between intracellular and extracellular environments [12].

Figure 3.3 shows the generalized form of excitable cell membrane equivalent circuit which is first claimed by Hodgkin and Huxley [11]. Kirchoff's law can be applied to this circuit due to the conservation of charge. Hence, the sum of capacitive current and total ionic transmembrane currents will be equal to zero as indicated by the equation referred to as Eq. 3.5.

$$C_m \times \frac{dE_m}{dt} = -(i_L + \sum_{j=1}^{N} i_j) \tag{3.5}$$

where C_m is the capacity of the membrane per unit area, E_m is the membrane potential, N is the total number of transmembrane currents, i_j is the j^{th} time-dependent transmembrane current, and i_L is the time-independent leakage or background transmembrane current [9].

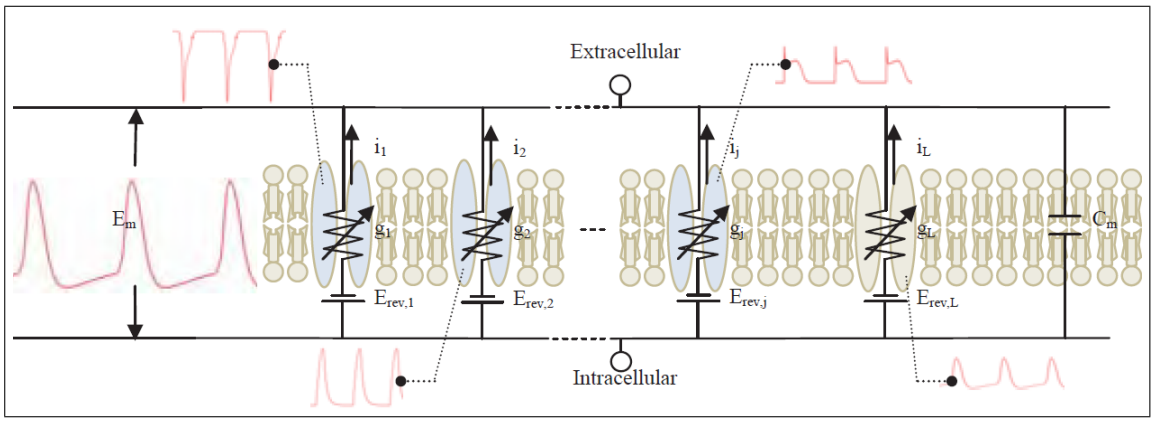

Figure 3.3 Generalized form of the electrical equivalent circuit for excitable cell membranes [9].

3.2 The Ion Channel Gating Concept

The electrochemical gradient is the major driving force behind the transmembrane ion fluxes which cause repolarization or depolarization of the plasma membrane. Some of the membrane proteins construct ion-selective channels in order to mediate these ion fluxes in a controlled manner [12]. Opening and closing of the transmembrane ion channels are controlled by a special gating mechanism which is first postulated by Hodgkin and Huxley in 1952. According to the postulation, each ion channel has a number of gates which control the transitions among open and closed conditions of the channel. The gating mechanism completely relies on the membrane potential [11]. Each of the transmembrane ion channels can be thought of as a tunnel which has a number of sequenced gates on it as illustrated in Figure 3.4. If these gates are open all at once, just then the channel allows the ion flow through it. Therefore the channel will be closed even only one of the gates is closed within it.

The shift among open and closed positions of the individual gates is a stochastic and rapid process. The membrane potential is the main factor in determining the channel gate's open probability. From the molecular point of view, the channel gates can be thought as tiny charged particles which translocate within the channel based on the actual membrane potential. These molecular translocations can occlude the ion channel to prevent the ion flow and *vice versa*. Each ion channel can have different

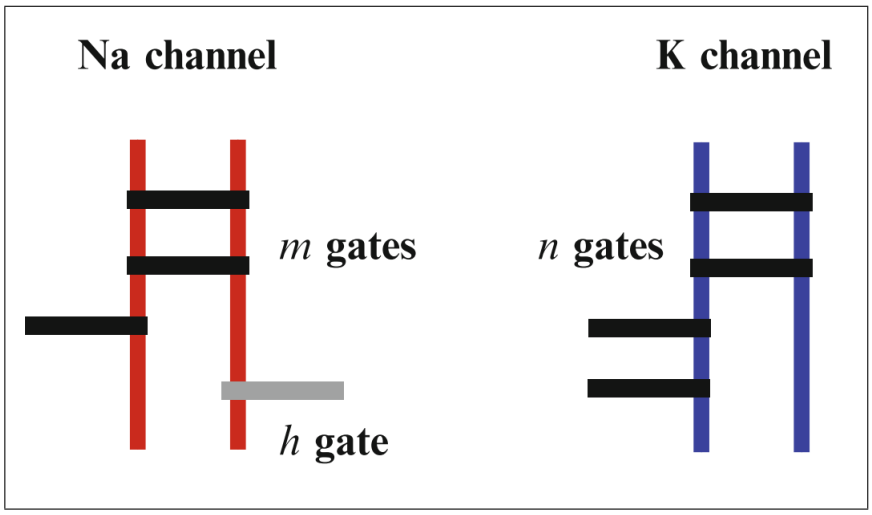

Figure 3.4 Graphical representation of gates opening and closing within the channels [10].

numbers of gates with different characteristics.

The gates of the ion channels can be classified into two groups. One of them is the activation gates group which has an open probability in direct proportion to depolarization. On the other side, the other one is the inactivation gates group which responds to depolarization with a decrease in open probability. Activation variable describes the open probability of a gate at any point in time. The open portion of total gates in the same class can be defined by the activation variable. Additionally, activation variable depends on the electrical potential of the membrane. The alteration rate of the activation variable based on the actual membrane potential is characteristic to each gate class [54].

α and β parameters shown in Figure 3.5 are named as the rate constants of the shift among closed and open positions of channel gates. α indicates the rate at which the gates in the closed state open while β describes the transition rate from open to the closed state.

Let's assume that a proportion of a gate population P is in the open state and the value of P is in the interval from 0 to 1, then the remaining portion $(1 - P)$ will be in the closed state. Thus, the amount of the gates opening and closing at any time

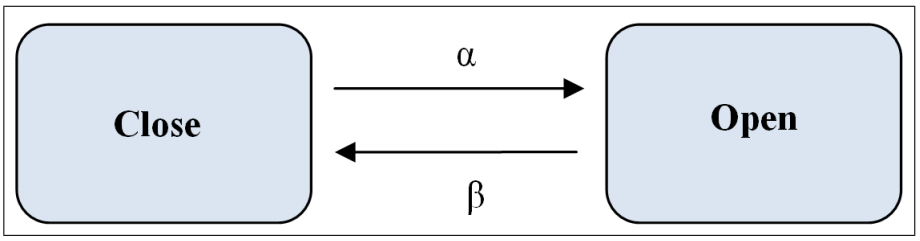

Figure 3.5 Transition between open and closed states.

can be expressed as Eq. 3.6 and Eq. 3.7, respectively.

$$Y_1 = \alpha \times (1 - P) \tag{3.6}$$

where Y_1 indicates the number of gates shifting from the closed position to open position, α is the voltage-dependent rate constant for this transition, and $(1 - P)$ is the number of gates in the closed state at a given time.

$$Y_0 = \beta \times P \tag{3.7}$$

where Y_0 is the number of gates shifting from open position to closed position, β is the voltage-dependent rate constant for this transition, and P is the number of gates in the open position at a given time.

In the equilibrium condition of the system, the number of gates closing should be equal to the number of gates opening at a given time period. Thus,

$$\alpha \times (1 - P) = \beta \times P \tag{3.8}$$

which can be rearranged as,

$$P_{\infty} = \frac{\alpha}{\alpha + \beta} \tag{3.9}$$

where P_{∞} indicates stochastic state of the gates when the system attains equilibrium condition with stable rate constants of transition for a certain time period. To exemplify, if β is higher than α, the gates will have a higher probability of being in the closed position, and *vice versa*.

The transition rate constants α and β are voltage-dependent and their values change based on the membrane potential value. Moreover, the probability of being open or closed for a specific group of gates also change with alterations of the membrane potential. Two groups of gate exist in the Hodgkin and Huxley formalism which are activation and inactivation gates. The opening probability of activation gates increases with depolarization while this probability decreases with depolarization for the inactivation gates. Instantaneous change of α and β ends up with a new value of P after a while [54]. P attains the new value at a rate of,

$$\frac{dP}{dt} = \alpha \times (1 - \beta) - \beta \times P \tag{3.10}$$

where the right side of the equation indicates the difference between closing and opening rates. The solution of the differential equation Eq. 3.10 can be expressed as,

$$P = P_{\infty} - (P_{\infty} - P_{init}) \times e^{\frac{-t}{\tau}} \tag{3.11}$$

where P_{init} is the initial equilibrium value of P after an extended period of time with stable membrane potential, P_∞ is the new value of equilibrium following the change of the membrane potential, and τ stands for the time constant which can be calculated by,

$$\tau = \frac{1}{\alpha + \beta} \tag{3.12}$$

Furthermore, the transition rate constants α and β can be denoted in terms of τ and P_∞ through merging the equations Eq. 3.12 and Eq. 3.9. Hence, the new expressions can be referred to as Eq. 3.13 and Eq. 3.14.

$$\alpha = \frac{P_\infty}{\tau} \tag{3.13}$$

$$\beta = \frac{1 - P_\infty}{\tau} \tag{3.14}$$

3.3 The Hodgkin-Huxley Formalism

Hodgkin and Huxley performed voltage clamp experiments in order to investigate the AP generation and propagation mechanisms in a giant axon of a squid. As a basic conceptual approach, they conducted measurements of membrane currents required to stabilize the potential of the cell membrane at a constant level instead of observing the membrane potential alterations in the course of an AP. In order to achieve this, an electrode is placed inside the squid axon and the cell is excited. A set of currents is applied across the cell membrane to prevent the alterations in the

membrane potential. Amplitude and timing of the transmembrane currents are quantified through the applied current measurements. Hodgkin and Huxley divided the total transmembrane ionic current into three components which are potassium current (I_K), sodium current (I_{Na}), and leakage current (I_l) which is made up of chloride and the other negatively charged ions [11].

Total transmembrane current flow I_i shown in Figure 3.6 is calculated by,

$$I_i = I_{Na} + I_K + I_l \tag{3.15}$$

where I_{Na}, I_K, and I_l stand for sodium, potassium, and leakage transmembrane currents, respectively.

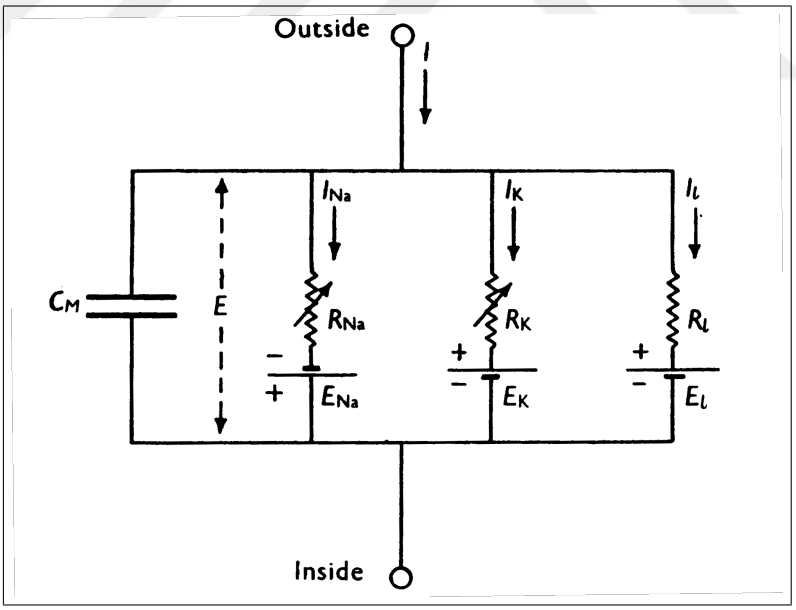

Figure 3.6 Electrical equivalent of the squid giant axon [11].

The individual membrane currents can be expressed as,

$$I_{Na} = g_{Na} \times (E_m - E_{Na}) \tag{3.16}$$

where g_{Na} is the conductance of Na^+ ion channel, E_{Na} is the equilibrium potential for Na^+ ions, and E_m is the actual transmembrane potential of the cell.

$$I_K = g_K \times (E_m - E_K) \tag{3.17}$$

where g_K is the conductance of K^+ ion channel, E_K is the equilibrium potential for K^+ ions.

$$I_l = g_l \times (E_m - E_l) \tag{3.18}$$

where g_l is the conductance of leakage current related ion channel, E_l is the equilibrium potential for leakage ions (chloride and others).

Concentration difference of a compound or ion between intracellular and extracellular environments generates chemical energy while the charge difference creates electrical energy. The electrochemical gradient due to these simultaneous differences induces potential energy on the cell membrane. If both of the electrical energy and the chemical energy are the same in amplitude with the opposite signs, the total ion flow would be equal to zero due to the cancellation of each other. This situation is called as electrochemical equilibrium and the membrane potential in this condition is named as equilibrium potential. The driving force for the transmembrane ion flow is created by the equilibrium potential [20].

Hodgkin and Huxley postulated that the potassium channel contains four activation gates which have open probability increases in direct proportion to depolarization. Thus, the channel's open probability will be n^4 where n represents the open probability of one activation gate for potassium channel. Assuming that open probability of one

n-gate is 0,5 at a specific membrane potential, then the whole potassium channel would have the open probability of 1/16 which means that every 1 potassium channel of 16 will be open in a whole population of potassium channels. Hence, the membrane's actual potassium conductance can be calculated by,

$$g_K = n^4 \times G_{K_{max}} \tag{3.19}$$

where $G_{K_{max}}$ is the complete potassium conductance in the case all of the potassium channels are in the open position.

On the other side, the sodium channels possess three gates of activation (m-gates) and one gate of inactivation (h-gate) in the proposed model by Hodgkin and Huxley. Thus, the membrane's sodium conductance at any time can be expressed as,

$$g_{Na} = m^3 \times h \times G_{Na_{max}} \tag{3.20}$$

where $G_{Na_{max}}$ is the complete sodium conductance in the case all of the sodium channels are in the open position.

Eventually, the total membrane current I shown in Figure 3.6 can be calculated with the equation referred to as Eq. 3.21.

$$I = C_m \times \frac{dE_m}{dt} + I_i \tag{3.21}$$

where C_m is the capacity of the membrane, E_m is the electrical potential of the

membrane, I_i is the transmembrane ion current density, and t is time.

Additionally, the gating mechanism for the sodium channel is depicted in Figure 3.7. The channel is available to open in reaction to a depolarizing stimulus when it is in the closed-resting state. Depolarization increases the channel's open probability and causes activation from closed-resting state to open state. Moreover, it causes the channel to fall into the refractory condition. Nevertheless, the initial response will be opening of the channel due to the fact that activation occurs more quickly than inactivation. The slower inactivation process closes the channel after a while which ends up with the closed-inactive condition of the channel. Recovery or reactivation from closed-inactive state to closed-resting state occurs when a further stimulus is applied [19]. In the cardiac myocytes, repolarizing outward potassium currents restore the membrane potential to its resting value which reactivates the calcium and sodium channels [12].

As a general principle in regulation mechanisms of biological systems, a signal which initiates a quick response also triggers a slower counter-process in order to terminate this response and avoid the runaway signaling [19].

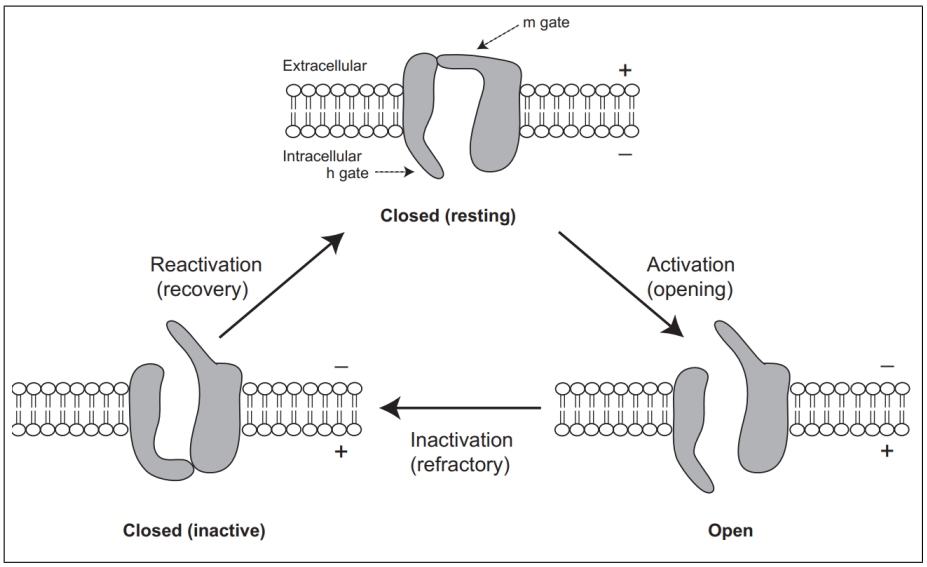

Figure 3.7 Gating cycle for the sodium channel. Movements of the m gate control the opening of the channel while h gate movements modulate the reactivation and inactivation processes [12].

3.4 Roots of the Cardiac Cell Modeling

Hodgkin and Huxley created a giant leap in terms of modeling the excitable cells with their seminal work published in 1952. They conducted several experiments on a squid's axon and came up with a novel mathematical model which describes the ion channel kinetics and predicts the AP characteristics such as shape, the velocity of conductance, and impedance alterations correctly [55]. The key success of the Hodgkin and Huxley's approach arose from combining the physics of electrical current flow with the reaction theory related to conformational changes within the ion channels. This approach differed from Cole's which was purely physical and first published in 1939. Cole noticed that it was not efficient enough to represent the cell membrane of a nerve through resistors, batteries, and capacitor. The lack of inductive behavior was the problem and an inductor was included in the representation of the cell membrane. Nevertheless, this approach did not properly reflect the molecular kinetics of the ion channels. Yet, at that time existence of the ion channels was not clear and studies about electrical properties of the nerve membrane were in progress. Basically, Hodgkin and Huxley's foresighted approach to combine the electrical description of the current flow with conformational change kinetics of ion channels from the molecular biology point of view was the crucial factor of their success. Moreover, they made an excellent choice by choosing the giant axon of the squid to experiment with due to the fact that it is one of the simplest excitable cells in comparison with more complex ones such as cardiac cells. Ironically, Cole sent a letter to Denis Noble with a book gift in which he wrote "Nerve has been so tedious. How can the heart be much more difficult ?" [21].

Electrical activity in the nerve cell differs from one in the cardiac cell on several counts. First of all, the APD for a nerve cell is about 1 ms and frequencies can go up to 1 kHz. On the other side, ventricular APD is about 400 ms in the heart and frequencies change around 1 Hz [33]. The longer duration and slower frequency mean that several ionic events occur in one AP cycle for controlling the contractility of the heart properly. Thus, cardiac cells have more complex mechanisms underlying AP generation and conduction in comparison with the nerve cells. Accordingly, this complexity leads to more detailed mathematical models for cardiac cells even the same

Hodgkin and Huxley formalism is utilized.

In 1960, Otto Hutter and Denis Noble showed that the Purkinje fibers have two types of potassium channels which are the delayed and the inward rectifier channels. A few years later, Noble attempted to adopt the Hodgkin and Huxley's formalism for developing a cardiac AP model. Therefore, he used the same Hodgkin-Huxley (HH) equations for the sodium current and slowed-down version of the HH potassium current equations to describe the delayed rectifier current in his model. Moreover, he fitted his own equations for the inward rectifier current [55]. Consequently, he came up with the very first cardiac cell membrane model as shown in Figure 3.8 which describes the AP generation kinetics in Purkinje fibers with four ODEs [1].

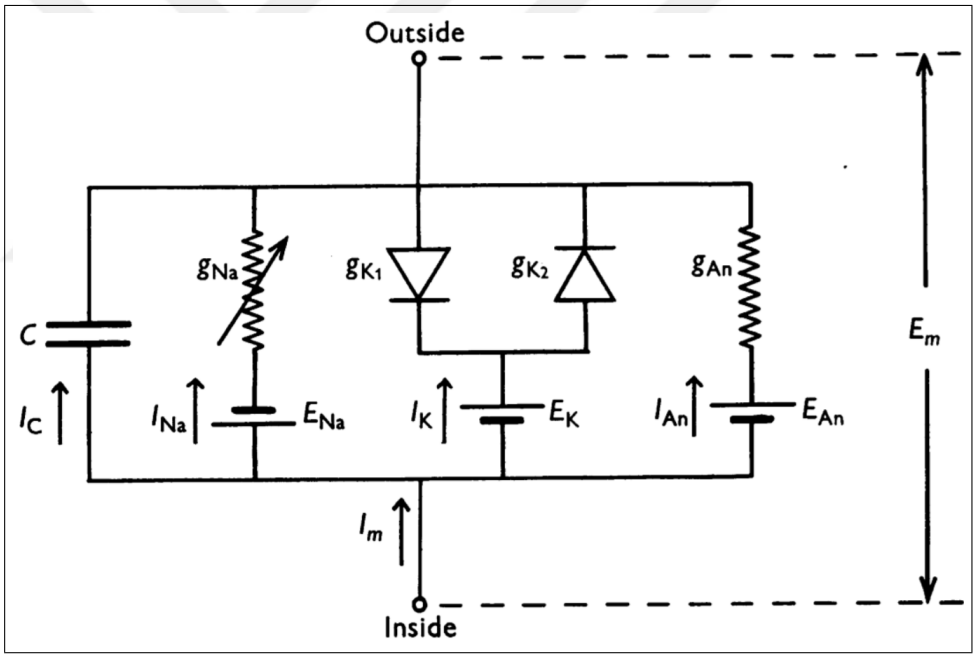

Figure 3.8 Electrical equivalent circuit of the Purkinje cell membrane which is claimed by Noble in 1962. The only difference is the assumption of two nonlinear resistances g_{K1} and g_{K2} for potassium current flow in comparison with the HH model for squid axon membrane. g_{K1} decreases with the membrane depolarization while g_{K2} slowly increases with it [13].

In the 1960s three major advancements occurred related to the cardiac cell modeling. Firstly, Reuter discovered the calcium current in the Purkinje fibers of the heart and published this work in 1967. Dick Tsien found out that slow potassium current alterations possess multiple components. Consequently, these two achievements resulted in the growth of McAllister-Noble-Tsien (MNT) Purkinje fiber model. This

model created a basis for the very first ventricular cell model created by Beeler and Reuter (BR) in 1977. The other significant advancement at that time was the discovery of sodium-calcium exchange in cardiac muscle cells which was discovered and published by Reuter and Seitz in 1969 [55]. The early mammalian cardiac cell models (1960-1989) are listed in Table 3.1, Table 3.2, and Table 3.3.

Table 3.1
Early models of mammalian Purkinje fiber cell [20].

Model	Predecessor Model
Noble	-
McAllister et al.	Noble
DiFrancesco and Noble	McAllister et al.

Table 3.2
Early models of mammalian ventricular cell [20].

Model	Predecessor Model
Beeler and Reuter	McAllister et al.
Drouhard and Roberge	Beeler and Reuter

Table 3.3
Early models of mammalian AVN and SAN cells [20].

Model	Predecessor Model
Hilgemann and Noble	DiFrancesco and Noble
Yanagihara et al.	-
Irisawa and Noma	Yanagihara et al.
Bristow and Clark	McAllister et al.
Noble and Noble	DiFrancesco and Noble
Noble et al.	Noble and Noble

3.5 The First and The Second Generation Cardiac Cell Models

The early models of cardiac cells were quite simple as they were containing a small number of differential equations and variables. Also, they were lack of formulations related to ion concentration regulation mechanisms. Thus, several ion concentrations were held constant in the model descriptions. These early type models are named as the first generation models.

The lack of enough experimental data and sufficient computational power caused a jog-trot between 1960 and 1990 [33]. Huxley stated in his Nobel lecture, "this was a laborious business: a membrane action took a matter of days to compute, and a propagated action potential took a matter of weeks". In the 1960s when Noble created the first cardiac cell model for Purkinje fiber, he wrote a computer program in machine code to solve the differential equations of the model. Even the equations were containing just five variable, it took about two hours to solve the equations for a single AP period [20]. In subsequent years the computational power has increased exponentially and since 1990 there has been a remarkable explosion of cardiac cell modeling work [33]. The progress in experimental cardiac electrophysiology and availability of powerful computing tools have been leading to more complex and detailed cardiac model developments. The second generation models are more realistic in terms of physiological details. They contain several ODEs and variables to describe the AP characteristics correctly. Moreover, they usually support the simulations of ion concentration kinetics instead of holding them fixed.

The diversity of cardiac cell models arose from the compromise between computability and complexity. For instance, calcium dynamics of cardiac cells consist of complex processes and including these dynamics into the model can make it computationally ineffective. Thus, if the model contains a higher level of physiological details, it will become hard to use especially for large-scale multicellular simulations due to the demand for high computational power [33]. The brief descriptions of ground-breaking cardiac cell models are listed in Table 3.4, Table 3.5, and Table 3.6.

Table 3.4
Ground breaking cardiac cell models - 1 [21].

Model	Type	Species	ODEs	Comments
Noble, 1962	Purkinje	Mammalian	4	First cardiac cell model.
Krause et al. 1966	Ventricle	Mammalian		First ventricular cardiac cell model.
McAllister et al. 1975	Purkinje	Mammalian	10	Introduction of repolarising potassium currents and second-inward calcium current. First use of experimental data to derive rate equations.
Hunter et al. 1975	Purkinje	Mammalian	1	Polynomial model with a single variable.
Beeler and Reuter, 1977	Ventricle	Mammalian	8	First well-used mammalian ventricular model.
Beeler and Reuter, 1977	Ventricle	Mammalian	8	First well-used mammalian ventricular model.
Yanagihara et al. 1980	SAN	Mammalian	7	First SAN model.
DiFrancesco and Noble, 1985	Purkinje	Mammalian	16	Introduction of the sodium - calcium exchanger, ionic concentrations, etc.
Hilgemann and Noble, 1987	Atrium	Rabbit	15	First atrial model and revolutionized calcium dynamics.
Rasmusson et al. 1990a	Atrium	Frog	16	First, and only, frog atrial model.
Rasmusson et al. 1990b	SAN	Frog	14	First, and only, frog SAN model.
Luo and Rudy, 1991	Ventricle	Guinea pig	8	First guinea-pig ventricular model (with Noble et al. 1991).
Noble et al. 1991	Ventricle	Guinea pig	17	First guinea-pig ventricular model (with Luo and Rudy, 1991).
Winslow et al. 1993				First network models.
Endresen, 1997	SAN	Mammalian	3	Simplification.

Table 3.5
Ground breaking cardiac cell models - 2 [21].

Model	Type	Species	ODEs	Comments
Fenton and Karma, 1998	Ventricle	Mammalian	3	Simplification with just three membrane currents.
Jafri et al. 1998	Ventricle	Guinea pig	31	Introduction of mechanistic calcium dynamics into the Luo and Rudy models.
Noble et al. 1998	Ventricle	Guinea pig	22	Introduction of the dyadic space for calcium, repolarizing potassium currents, persistent sodium current, stretch and drug effects.
Priebe and Beuckelmann, 1998	Ventricle	Human	22	First human ventricular model. Introduced formulations for the normal and failing hearts.
Winslow et al. 1999	Ventricle	Canine	33	First canine ventricular model.
Ramirez et al. 2000	Atrium	Canine	25	First canine atrial model.
Bondarenko et al. 2004	Ventricle	Mouse	41	First mouse ventricular model.
Iyer et al. 2004	Ventricle	Human	67	Joint first human ventricular model with Markov formulations for the fast sodium current, transient outward current, rapid delayed rectifier current and L-type calcium current.
ten Tusscher et al. 2004	Ventricle	Human	17	Joint first human ventricular model from human data.
Cortassa et al. 2006	Ventricle	Mammalian	50	Introduction of electrophysiology, contraction and mitochondrial bioenergetics together.
Aslanidi et al. 2009b	Purkinje	Canine	30	First canine Purkinje model from canine Purkinje data.

Table 3.6
Ground breaking cardiac cell models - 3 [21].

Model	Type	Species	ODEs	Comments
Inada et al. 2009	AVN	Mammalian	29	First, and only, AVN model.
Li et al. 2010	Ventricle	Mouse	36	Complete refit of mouse model from mouse data.
Sampson et al. 2010	Purkinje	Human	82	Human Purkinje model from more detailed human data.
Corrias et al. 2011	Purkinje	Rabbit		Refit of most ionic currents from rabbit Purkinje data.
Li and Rudy, 2011	Purkinje	Canine		Complete refit of canine Purkinje model from canine Purkinje data.
O'Hara and Rudy, 2011	Ventricle	Human	41	Substantially improved human-specific model accuracy using human data.

4. METHODS

4.1 Ventricular Cell Model Implementation

Ventricular arrhythmia is considered to be the first clinical symptom of SCD which is the most common lethal form of CVD. Preventive measures have critical importance for SCD due to its characteristics of sudden occurrence and high fatality level. Underlying mechanisms of arrhythmia formation should be well understood in order to develop effective prevention techniques [56]. A proper model which describes the electrophysiological dynamics of the cardiac cell is essential for cardiac arrhythmia modeling and simulation studies. Unfortunately, it is quite difficult to access non-failing or undiseased ventricular tissue of the human heart for experimental research. Hence, most of the ventricular cell models have been created on the basis of data obtained from cardiac cells of animals. On the other side, it is a well-known fact that arrhythmia mechanisms and AP characteristics (shape, duration, restitution, ion currents e.g.) are dependent on species. Thankfully, in recent years increasingly more data have been collected from human cardiac cells. A novel method of cloning and heterologously expressing human cardiac ion channels in another cell type provided a significant opportunity to gather voltage clamp data related to human cardiac ionic currents. As a result of these advancements, several human ventricular cell models have been developed [32].

Priebe and Beuckelmann (PB) announced the first mathematical model for human ventricular cells in 1998 (Figure 4.1). In general, they built the proposed model upon phase two model equations derived by Luo and Rudy for the guinea pig ventricular cell. They adjusted the formulations related to the major ionic currents including L-type calcium current, the transient outward and the inward rectifier potassium current, and also the fast/slow elements of delayed rectifier potassium current using the quite limited data from human ventricular cells at that time. Furthermore, they studied the electrophysiological consequences of HF using the model they developed [17].

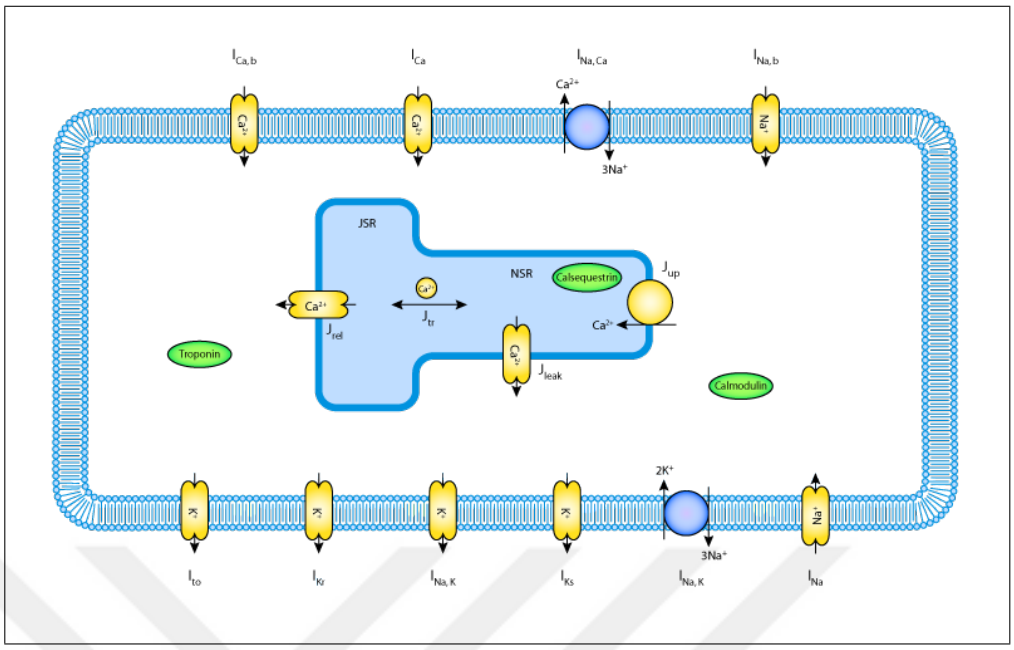

Figure 4.1 A schematic representation of the PB model which includes the descriptions of transmembrane ionic currents through pumps, exchangers, and channels. This model also describes the subcellular calcium handling mechanisms which makes it complex and computationally inefficient for large-scale simulations [14].

PB model is the second generation model which consists of several ODEs describing the time dependency of gating variables, membrane potential, and ion concentrations. The second generation models possess complications such as long term ion concentration drifts and degeneracy of equilibria which make them inherently unstable. Moreover, PB model is quite complex and computationally inefficient for especially large-scale simulations of arrhythmias. In 2002, Bernus et al. came up with a reduced version of the PB model (redPB) in order to overcome the limitations and reduce the complexity (Figure 4.2). They fixated the intracellular ionic concentrations and reduced the number of variables from 15 to 6 by reformulating some of the currents. Thus, the redPB model became more stable than the original model and also 4,9 times faster in terms of numerical computations [22].

The second generation cardiac cell models have intracellular ion concentration handling mechanisms which can be a reason for instabilities. PB model also shows such kind of instability with long term drifts of intracellular Na^+ and K^+ concentrations. Due to the fact that intracellular Na^+ and K^+ concentrations express minor variations

over the course of an AP, they are fixated to the values of 10 mM and 140 mM, respectively in the redPB model which are the initial values of related ions in the PB model. Furthermore, the intracellular Ca^{2+} concentration is adjusted as a constant value, 400 nM, to get rid of equations which describe the variations of intracellular Ca^{2+} concentration in the original PB model. These values can be changed through the graphical user interface (GUI) of developed simulation platforms in this thesis.

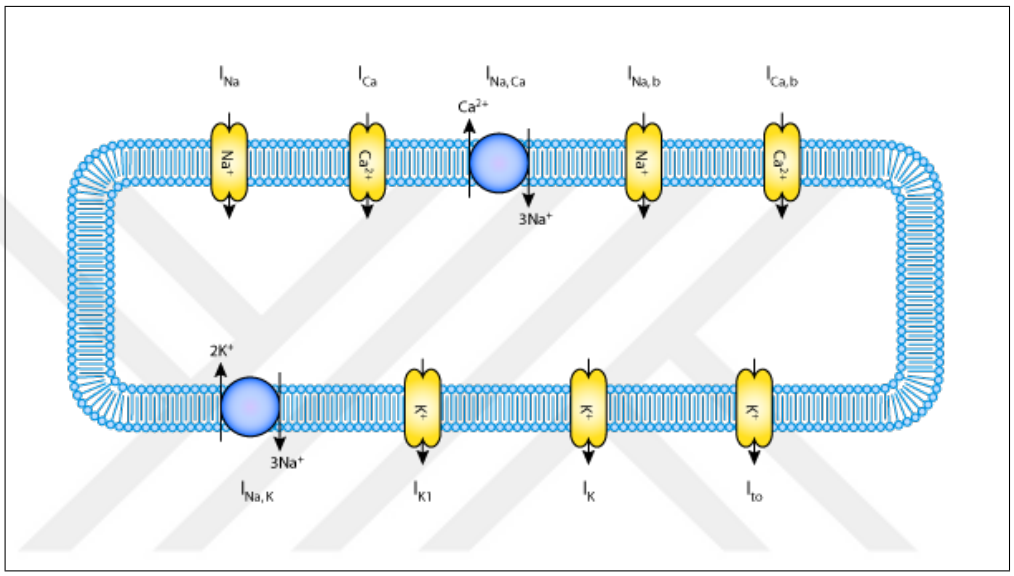

Figure 4.2 A schematic representation of redPB model which includes the descriptions of transmembrane ionic currents through pumps, exchangers, and channels. This model has fixated intracellular ionic concentrations differently from PB model [15].

The total transmembrane ionic current in the redPB model is described as,

$$I_{tot} = I_{Na} + I_{Ca} + I_{to} + I_K + I_{K1} + I_{Na,b} + I_{Ca,b} + I_{NaK} + I_{NaCa} \tag{4.1}$$

where I_{Na} is the fast sodium current, I_{Ca} is the calcium current, I_{to} is the transient outward potassium current, I_K is the delayed rectifier potassium current, I_{K1} is the inward rectifier current, I_{NaK} is the current generated by $Na^+ - K^+$ pump, I_{NaCa} is the current generated by $Na^+ - Ca^{2+}$ exchanger, $I_{Na,b}$ and $I_{Ca,b}$ are the background currents for sodium and calcium, respectively.

In this thesis, the redPB model is implemented in the developed simulation software due to its computational advantages. HF condition was investigated in the original PB publication however it was not studied with redPB model in the paper published by Bernus et al. One of the aims of this thesis is to show if it is possible to generate the same electrophysiological consequences of HF using the redPB model in a computationally more efficient way.

4.2 Software Development Tools

In this thesis, two cardiac AP simulation platforms are designed and developed. In the first one, MATLAB App Designer is utilized as an application development tool and just the redPB model is implemented. The second one is designed as a more general simulation software to allow simulations using a variety of cardiac cell models with a user-friendly GUI. This one is written in Python using the Myokit Application Programming Interface (API).

MATLAB is a fourth-generation general programming language created by MathWorks in order to allow matrix manipulations, algorithm implementations, plotting data/function graphs, creating user interfaces, and interfacing with programs written in other languages. It provides high-performance data analysis, numerical computation, and visualization opportunities for the users [57]. Hence, it has been frequently utilized in a variety of engineering and scientific studies all over the world.

MATLAB allows users to design user-friendly GUIs on top of its computational power with high-level script language capabilities. GUI applications can work independently from the operating system and enable the user interactivity [58]. The object-oriented programming (OOP) paradigm is implemented in 2007 in order to enable access to the advantages of OOPs such as encapsulation, inheritance, polymorphism and abstraction [57]. GUIDE is the well-known classical tool of MATLAB used for developing GUIs. In this thesis, App Designer is utilized instead of GUIDE which is a brand new GUI design tool firstly introduced in R2016a version of MATLAB. App

Designer allows users to develop modern, full-featured applications using a rich set of GUI components and custom interactions. Furthermore, it gives the opportunity to create standalone desktop applications and share them with other users. MATLAB has an online application repository which contains a variety of apps developed by the users around the world. Currently, it does not contain a simulation app for cardiac AP.

The second platform is designed as a more general cardiac AP simulation software which will enable users to import a variety of cardiac cell models and conduct simulations by using them easily. This software is written in Python which is an interpreted, object-oriented, and interactive programming language with expressive syntax such an executable pseudocode [59]. It is a remarkably powerful and yet popular programming language as ranked at the top among the other programming languages in 2018 [60]. The kernel of the Python is quite small and it can be extended through various extension modules which are referred to as packages. The distribution comes with a number of libraries containing standard packages. Furthermore, the user community of Python consists of members who develop and distribute a substantial number of packages for various applications [61]. Myokit is an open-source framework written predominantly in Python for computational cellular electrophysiology. The Myokit API provides several tools for tasks related to simulation and analysis. Moreover, it utilizes an easy-to-read model description language which enables users to edit the model files with any text editor and share them with other users in an easy way [62]. Hence, the Myokit API is utilized in the software development process for the backend of the software.

4.3 Simulation of Drug Effects

Effects of the channel blocker drugs such as tetrodotoxin (TTX), 4-aminopyridine (4-AP), and the exchanger inhibitory peptide (XIP) can be simulated using the Hill equation referred to as Eq. 4.2.

$$f(x) = \frac{1}{1 + (x/IC50)^h} \tag{4.2}$$

where x is the drug concentration to be applied, $IC50$ is the half-maximal value of inhibitory concentration, h is the Hill coefficient, and $f(x)$ is the maximum conductance scaling factor for the related channel. The value of the $f(x)$ can get values between 0 which means a full block of the channel and 1 which means no block [63].

User can calculate the $f(x)$ value for the drug to be applied using the Eq. 4.2 and enter the value as a percentage through the drug administration panel of the cardiac AP simulation app as shown in Figure 4.3.

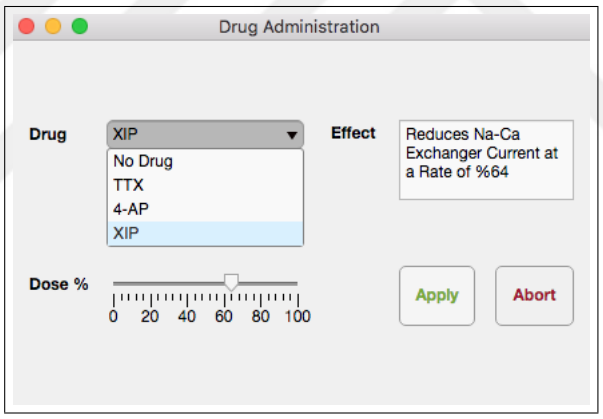

Figure 4.3 Drug Administration Panel.

5. RESULTS

This chapter explains the developed simulation platforms and introduces the cardiac action potential simulation results conducted on these platforms.

5.1 MATLAB Based Simulation Application

The first cardiac AP simulation platform is designed and developed on MATLAB using its brand new application development tool named App Designer. The redPB ventricular cell model is implemented in the application and the key parameters can be changed through the user-friendly GUI. Drug administration and HF condition options are also available. GUI of the application is depicted in Figure 5.1. The application can run as a standalone desktop application on any operating system that contains the MATLAB compiler.

Two fixed graph areas are positioned on the right side of the GUI in order to show the resulting plots of simulation. User can select the variables to be plotted on top and bottom graphs through the 'Graph Select' section on the left side. The previous simulation graphs can be held on by the 'Hold On' button and the next simulation graphs will be plotted on them with different colors. User can enter the parameters of the stimulus to be applied through the 'Stimulus Parameters' section. Frequency indicates the number of stimuli to be applied per second. Duration and amplitude of the stimulus can also be adjusted through this section. On the 'Ionic Concentration Parameters' section, extracellular and intracellular concentrations for major ions can be set prior to the simulation. Additionally, 'Simulation Parameters' section allows the user to determine the duration of simulation and the conditions to be applied during the simulation which are drug administration and HF. Green indicators show if the related condition is active or not.

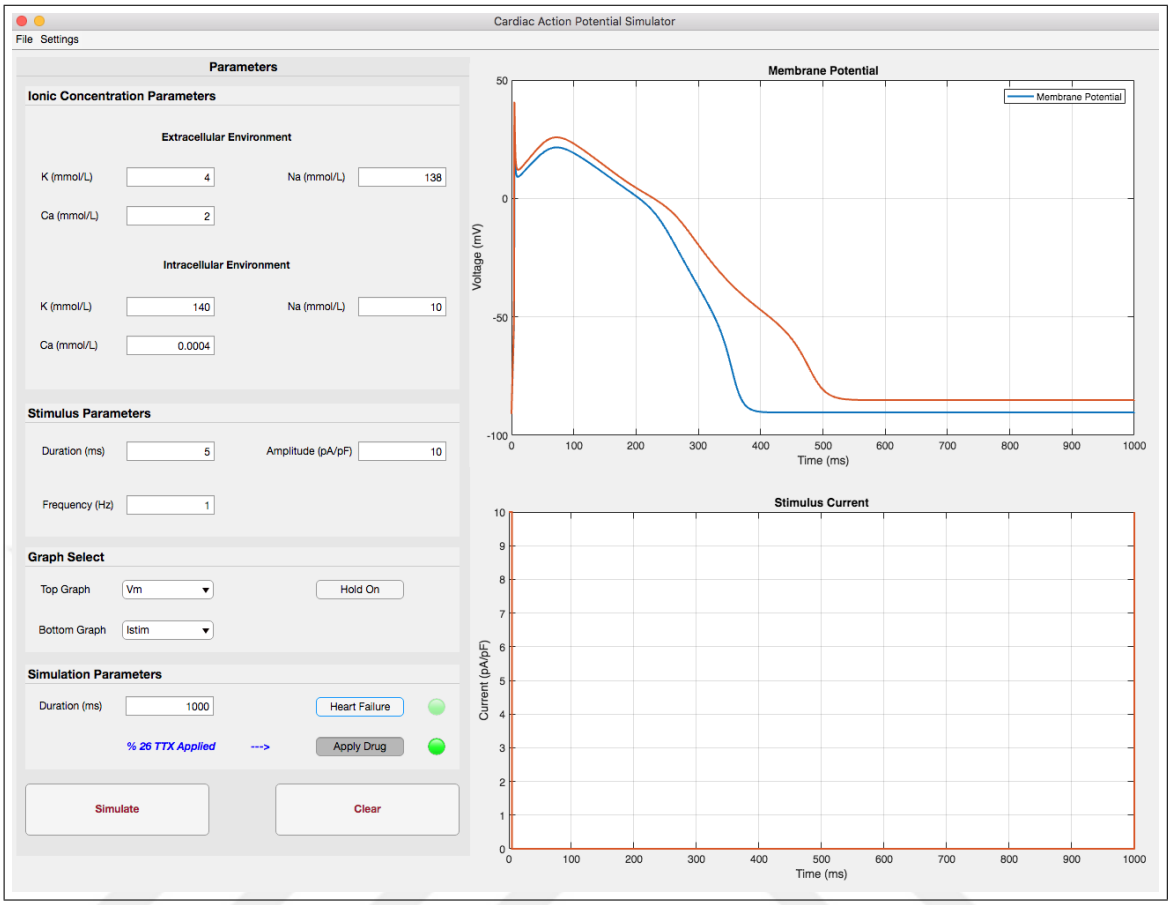

Figure 5.1 GUI of the Cardiac Action Potential Simulator.

When the user pushes the 'Apply Drug' button, a pop-up panel opens in order to let the user select the drug-related parameters as shown in Figure 5.2. Drug type and dose to be applied can be selected through this pop-up panel. The text area which is named as 'Effect' reflects the effect of the selected drug and dose. Moreover, when the user confirms drug administration on the pop-up panel through 'Apply' button, dose and type of the drug are shown on the main window near the 'Apply Drug' button with blue color (Figure 5.1). The button named 'Simulate' starts the simulation based on the parameters set before. The user can click the 'Clear' button in order to clear all graphs and restore all settings to default.

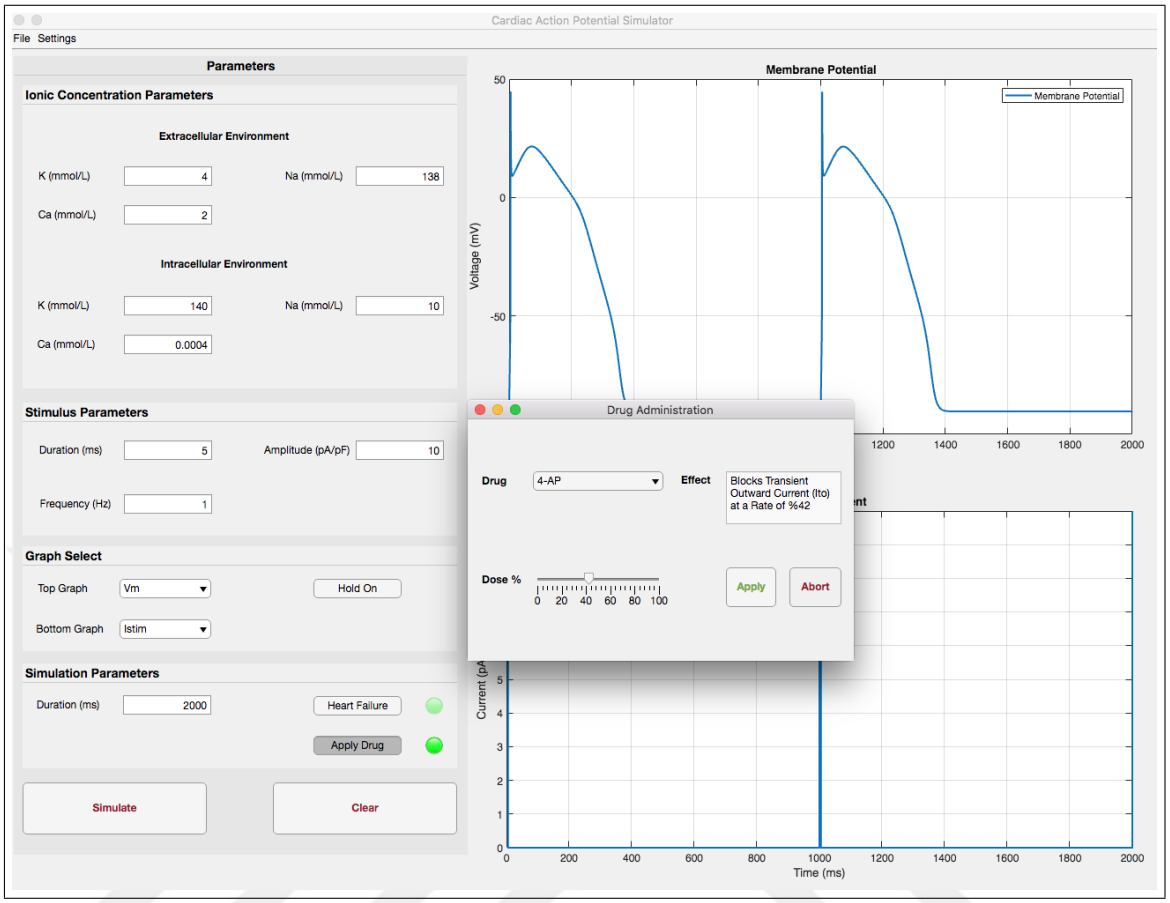

Figure 5.2 Pop-Up Panel for Drug Administration Parameters.

5.2 Cardiac Action Potential Simulator

The second cardiac AP simulation platform is written in Python and intended for simulations using a variety of cardiac cell models. The GUI is designed in Qt Creator and PyQtGraph library is utilized for plotting graphs. Simulations and model files are powered by the Myokit Python API.

The main window of the software consists of three tabs which are 'Action Potential', 'Graphics', and 'Parameters'. Figure 5.3 shows the GUI of the 'Action Potential' tab. First of all, the user can select a custom model definition file through 'Import Custom Model' section and 'Browse' button. Model files can be edited in any text editor and they should be saved with '.mmt' file extension. Myokit API enables more

human-readable and -editable model files than the XML based model languages such as CellML. Moreover, it is possible to get a model file written in CellML and convert it to the mmt file which will allow the user to import it to this software in order to conduct simulations. The PB model is implemented as a default model and 'Reset to Default' button restores all settings based on it. The user can edit extracellular and intracellular concentrations for major ions through the 'Ionic Concentration Parameters' section. Many of the model parameters are hidden from the user in order to make the GUI simple and user-friendly.

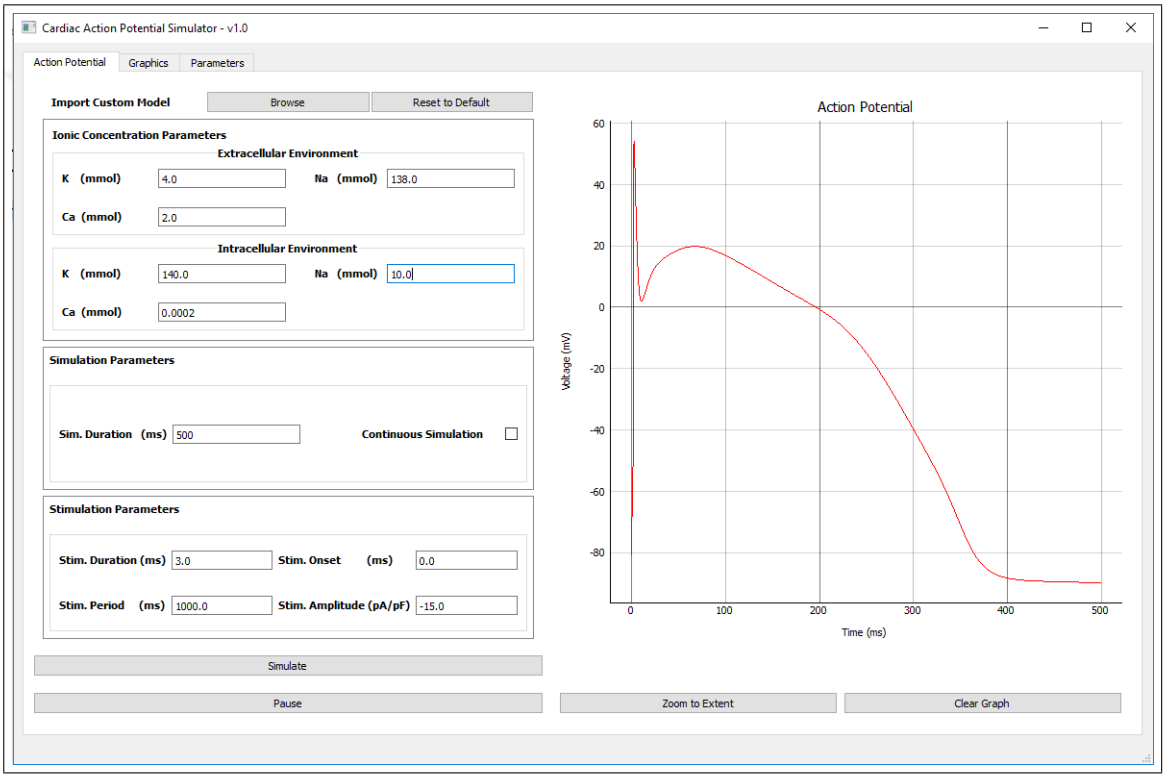

Figure 5.3 Main Window of the Cardiac Action Potential Simulator.

The duration of the simulation can be set through the edit box named 'Sim. Duration' which is in the 'Simulation Parameters' section. The simulation can be run continuously by putting a tick to the checkbox named 'Continuous Simulation'. If this option is selected, the stimulation will be applied consistently at a frequency based on the value in the edit box named 'Stim. Period' and the graph will flow left with a continuous plotting effect. The user can change the parameters during the continuous simulation and observe the subsequent effect of the change instantly on the graph.

Continuous simulation can be paused by the 'Pause' button. The characteristics of the stimulation to be applied are determined based on the values in the 'Stimulation Parameters' section. In this section 'Stim. Onset' stands for the time point when the stimulation will be applied. The duration of the stimulation can be set through the edit box named 'Stim. Duration'. Moreover, the amplitude of the stimulation current can be adjusted by the edit box named 'Stim. Amplitude'. The right side of the GUI is allocated for graph area which shows the result of simulation as the AP plot. The button named 'Zoom to Extent' enlarges the plot to fit into the graph area. The current plot can be cleared through the 'Clear Graph' button (Figure 5.3).

The 'Graphics' tab of the main window has a GUI as shown in Figure 5.4 and enables the user to plot further graphs related to the various parameters of the model used for simulation. The GUI is divided into two graph areas. Parameters to be plotted against the integration variable can be selected through the combo box widgets named 'Graph-1' and 'Graph-2' for left and right graph areas, respectively. Thus, the user can observe two graphs at the same time in order to compare them. Plots can be fitted into the graph areas through the buttons named 'Zoom to Extent'.

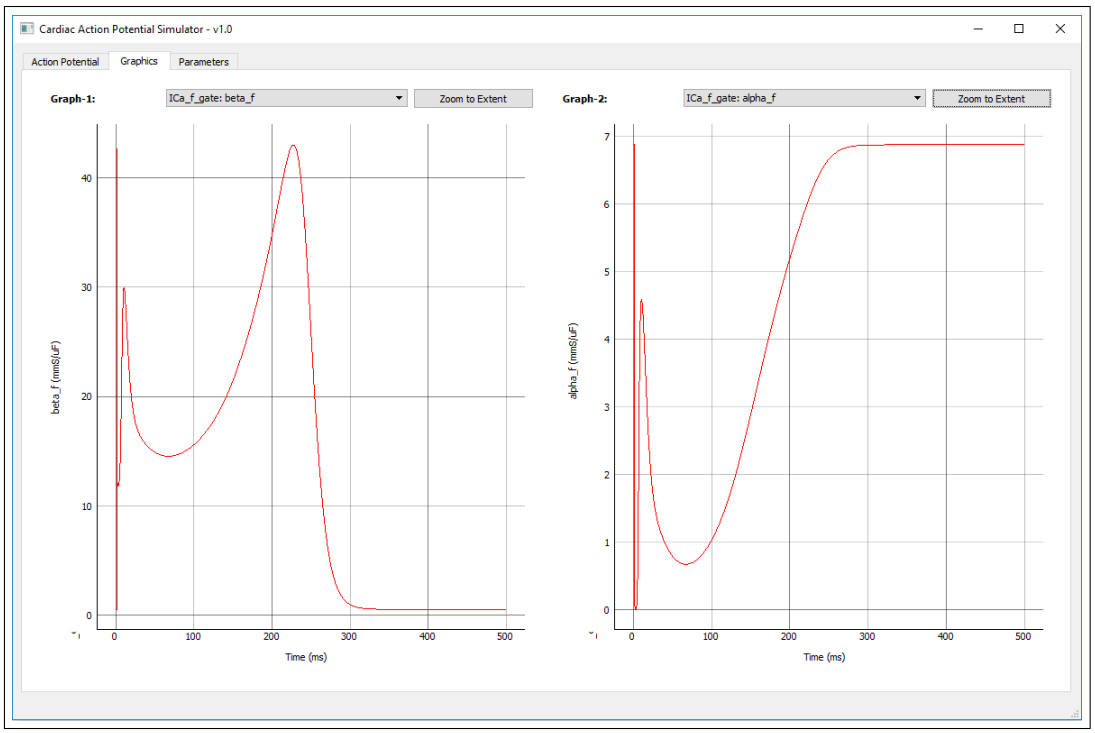

Figure 5.4 GUI of the Graphics Tab.

One of the main aims of this simulation software is to hide the complexity of the imported model from the user as much as possible. Therefore, 'Action Potential' tab of the main window allows editing just the main parameters of the model. On the other side, if the user would like to edit the further parameters, he/she can use the 'Parameters' tab as shown in Figure 5.5.

The 'Parameters' tab includes model constants such as maximum conductance of the channels and the constants related to the cell geometry. The user can edit these parameters through the edit boxes in the 'Constants' section.

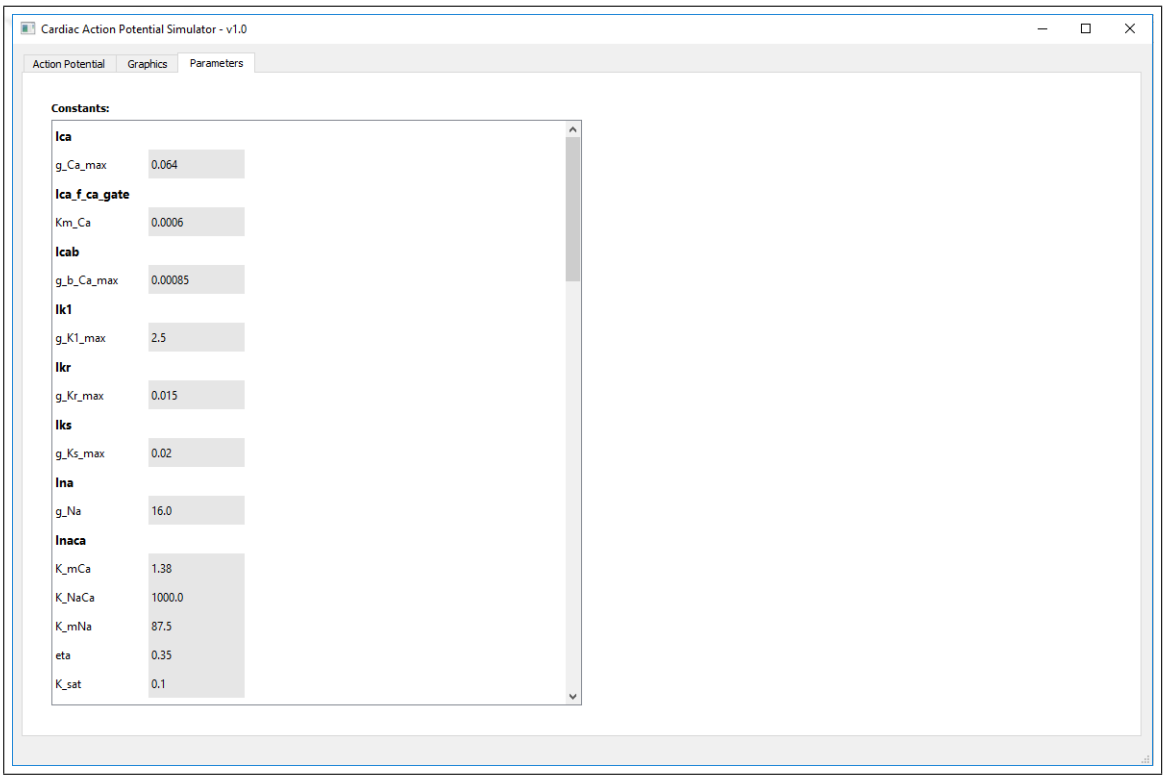

Figure 5.5 GUI of the Parameters Tab.

5.3 Simulation Results

Priebe and Beuckelmann introduced the first human ventricular cell model in 1998. PB model consists of 15 variables and it is a second-generation model as the ion concentrations and gating variables change over time [32]. Second-generation models

possess inherent complications such as ion concentration drifts in the long-term, the decay of equilibria, and instability. Bernus et al. reformulated some of the ion current equations in the PB model and came up with a reduced version in 2002. The redPB model has 6 variables and fixated intercellular ion concentrations [22]. Hence, it is a first generation human ventricular cell model with reduced complexity.

In this thesis, these two models, PB, and redPB, are implemented and several single cell simulations are conducted on them through the developed software and application. The simulation platforms run on a PC with an AMD Ryzen 3 2200G CPU.

5.3.1 Control Case

In this case, simulation is conducted using the PB and redPB models. The parameter values are set as claimed in the original papers for the healthy human ventricular cell. The simulation duration is adjusted to 2000 ms and stimulation current is applied at a frequency of 1 Hz with an amplitude of $-15\mu A$. As shown in Figure 5.6, AP shapes generated by the two models are quite similar. Simulation times are elapsed as 0,54 second for redPB model and 0,9 second for PB model. This outcome confirms the computational efficiency of the redPB model.

5.3.1.1 Fast Na^+ Current. In the PB model dynamic characteristic of the fast Na^+ current is represented by fast inactivation variable (h), slow inactivation variable (j), and very fast activation variable (m) as shown below

$$I_{Na} = g_{Na} \times m^3 \times h \times j \times (E_m - E_{Na}) \tag{5.1}$$

where g_{Na} is the maximum Na^+ channel conductance, E_m is the membrane

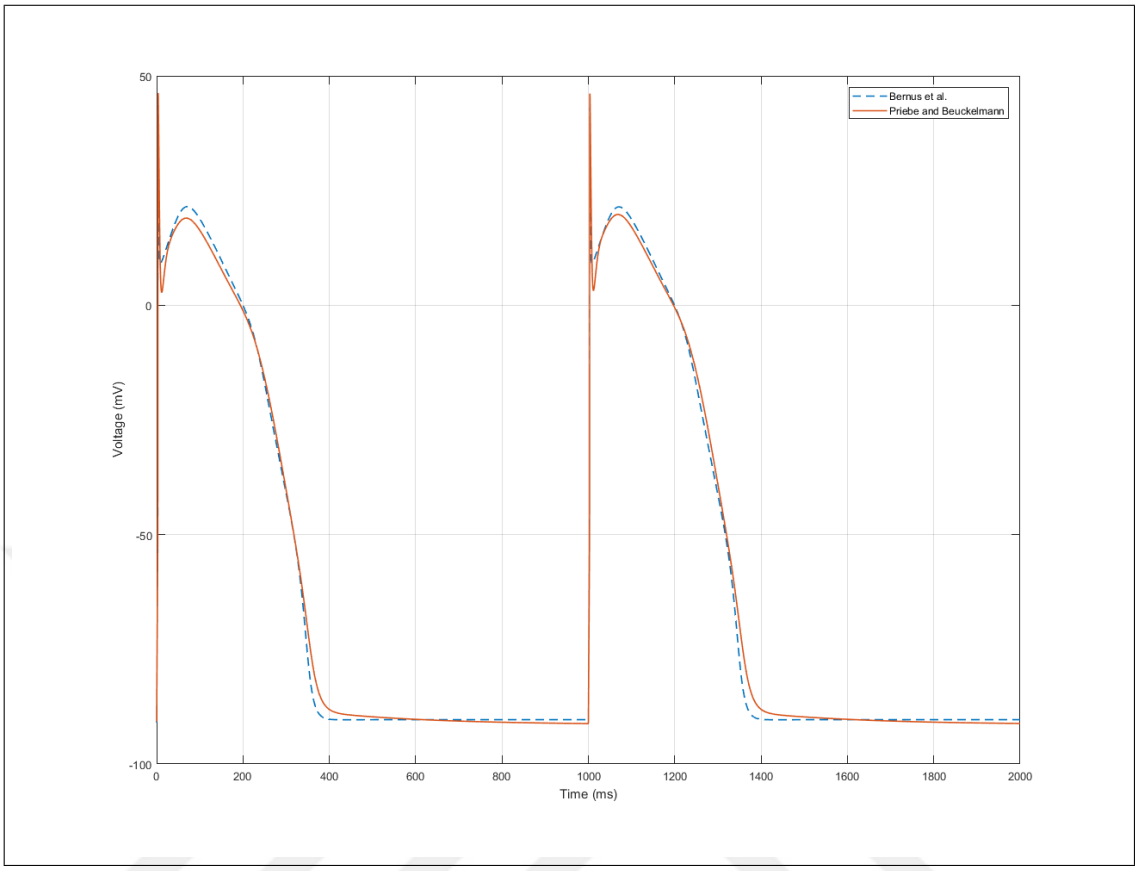

Figure 5.6 APs generated for healthy human ventricular cell using PB and redPB models.

potential, and E_{Na} is the Nernst potential for Na^+.

In the redPB model, the inactivation kinetic of I_{Na} is remodeled by multiplication of the two inactivation variables h and j. Thus, the I_{Na} equation became,

$$I_{Na} = g_{Na} \times m^3 \times v^2 \times (E_m - E_{Na}) \tag{5.2}$$

where v is the new inactivation variable.

Simulation results of I_{Na} can be observed in Figure 5.7 and Figure 5.8.

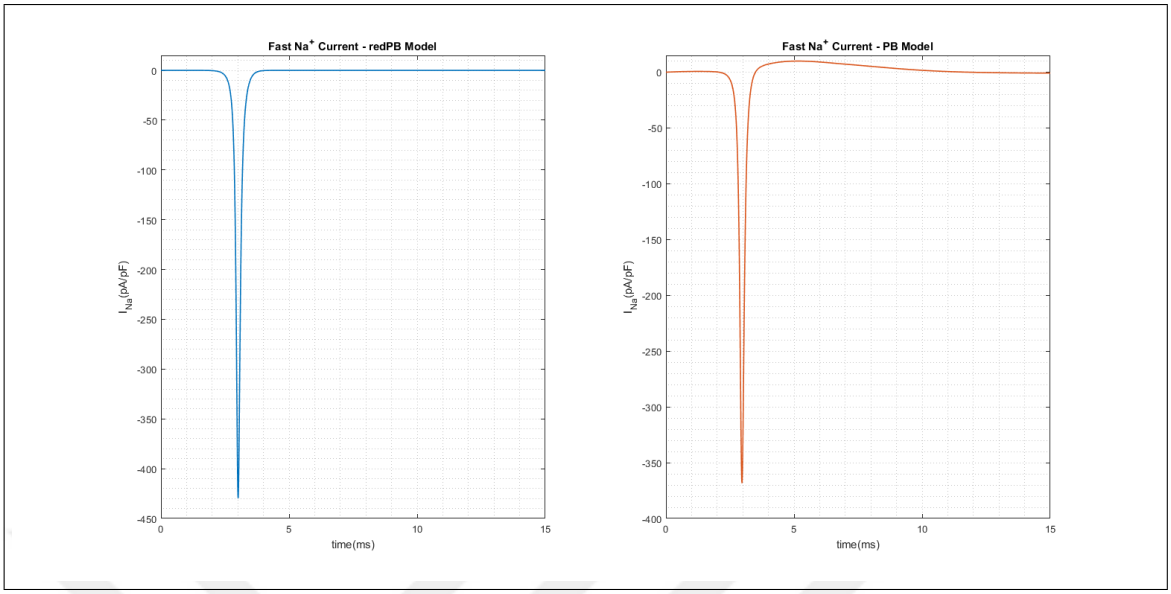

Figure 5.7 Fast Na^+ current for PB and redPB models.

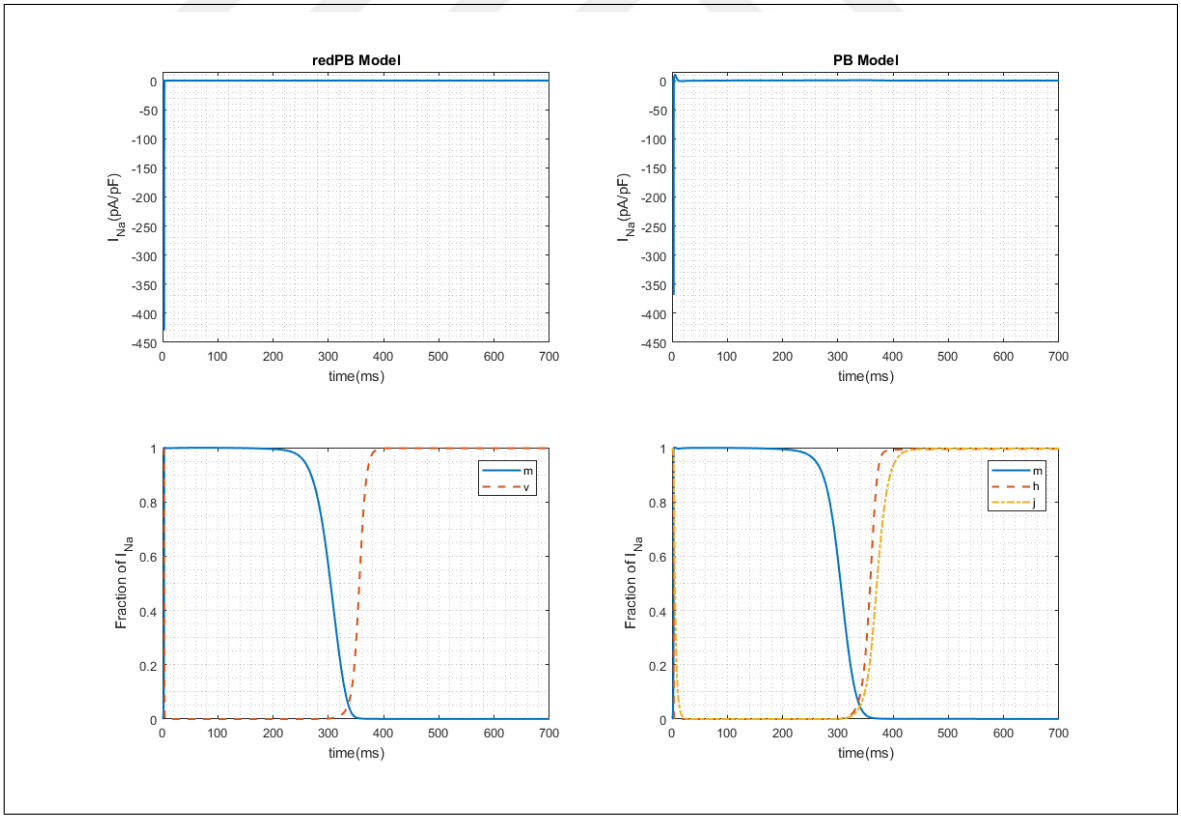

Figure 5.8 Fast Na^+ current and activation-inactivation variables for redPB and PB models.

5.3.1.2 Ca^{2+} Current. In the PB model I_{Ca} is described using the HH type activation and inactivation variables which are d and f, respectively. Additionally, Priebe and Beuckelmann implemented an E_m independent factor f_{Ca} for intracellular Ca^{2+} dependent inactivation.

The Ca^{2+} current is modeled as shown with Eq. 5.5 in the PB model.

$$I_{Ca} = g_{Ca} \times d \times f \times f_{Ca} \times (E_m - E_{Ca}) \tag{5.3}$$

where g_{Ca} is the maximum Ca^{2+} channel conductance and E_{Ca} is the Nernst potential for Ca^{2+}.

$$f_{Ca} = 1/(1 + [Ca^{2+}]_i/0.0006) \tag{5.4}$$

where $[Ca^{2+}]_i$ stands for the intracellular Ca^{2+} concentration.

In the redPB model the activation variable, d is eliminated due to the fast characteristic of the I_{Ca} activation. Also, the f_{Ca} factor became constant because of fixated intracellular Ca^{2+} concentration. Thus the reformulation of I_{Ca} is

$$I_{Ca} = g_{Ca} \times d_\infty(E_m) \times f \times f_{Ca} \times (E_m - E_{Ca}) \tag{5.5}$$

Simulation results of I_{Ca} can be viewed in Figure 5.9 and Figure 5.10.

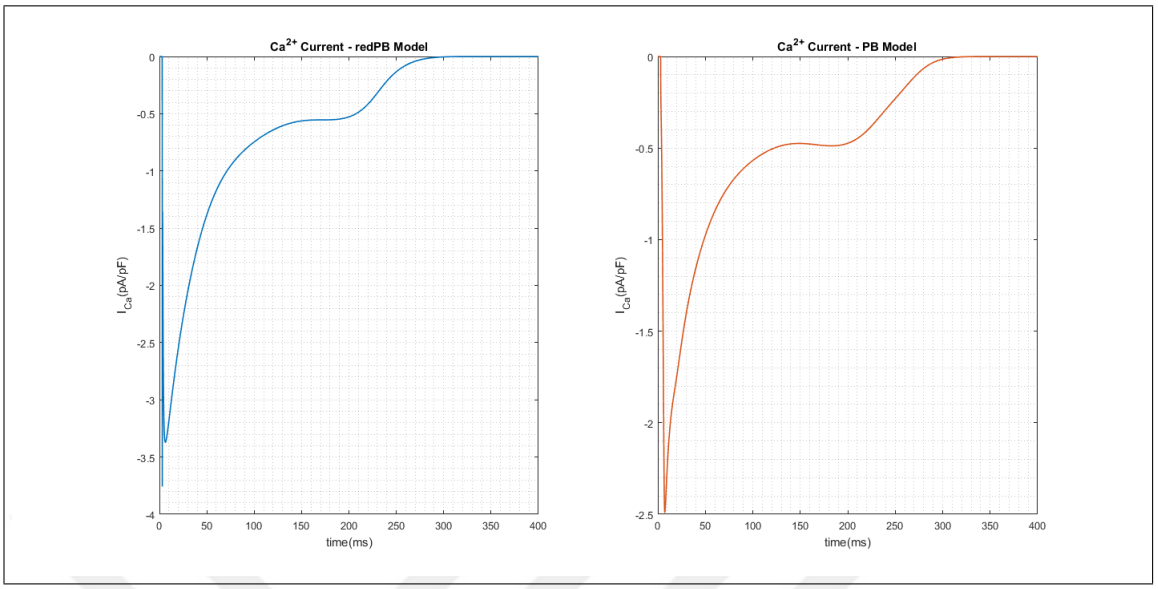

Figure 5.9 Ca^{2+} current for PB and redPB models.

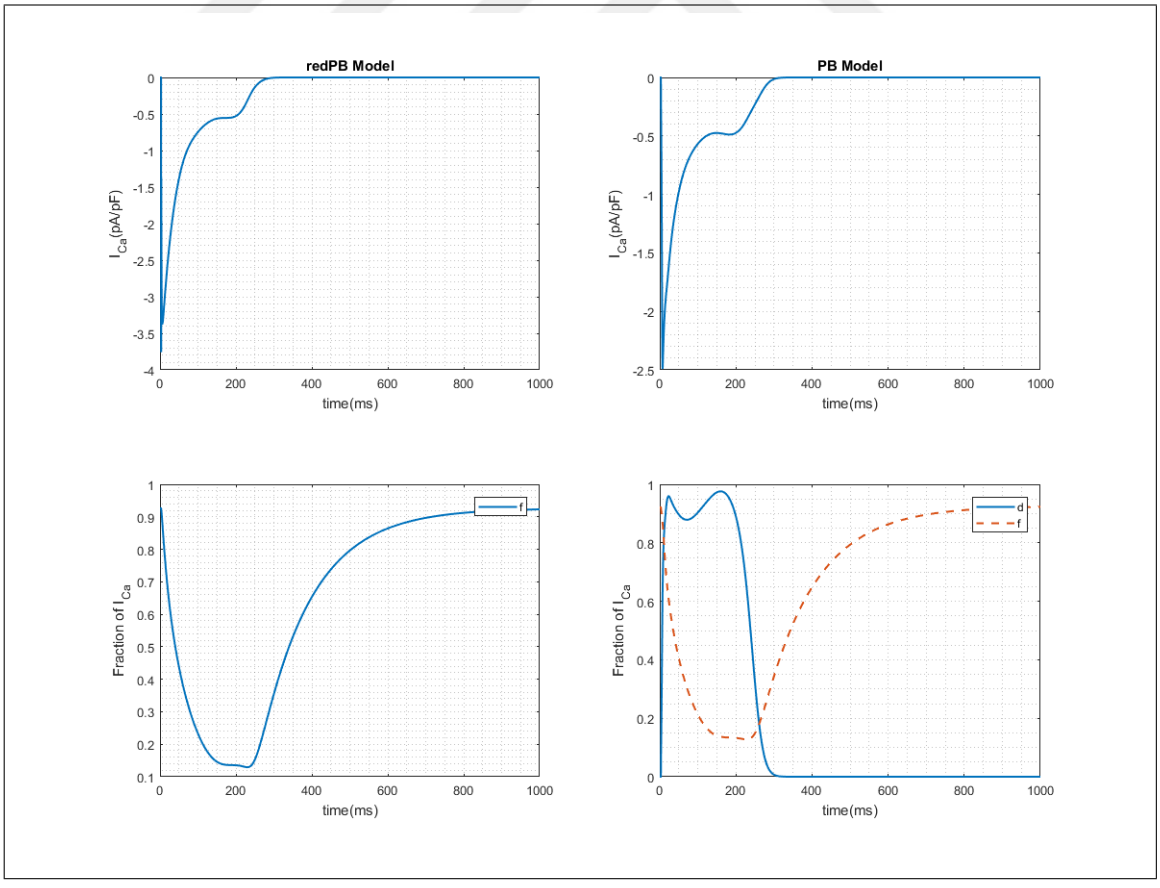

Figure 5.10 Ca^{2+} current and activation-inactivation variables for redPB and PB models.

5.3.1.3 Transient Outward K^+ Current. In the PB model transient outward current is described as,

$$I_{to} = g_{to} \times r \times to \times (E_m - E_{to}) \tag{5.6}$$

where g_{to} is the maximum transient outward channel conductance, to is inactivation variable, r is very fast activation variable, and E_{to} is the Nernst potential for transient outward current.

Bernus et al. eliminated the very fast activation variable, r adiabatically and reformulated the transient outward current as shown below,

$$I_{to} = g_{to} \times r_{\infty}(E_m) \times to \times (E_m - E_{to}) \tag{5.7}$$

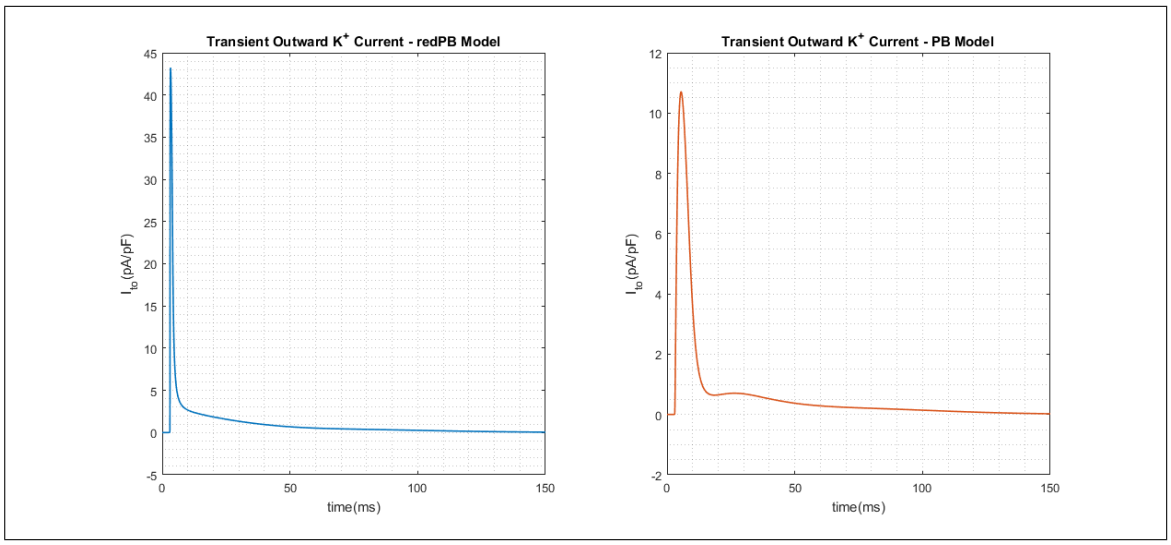

Figure 5.11 Transient outward K^+ current for PB and redPB models.

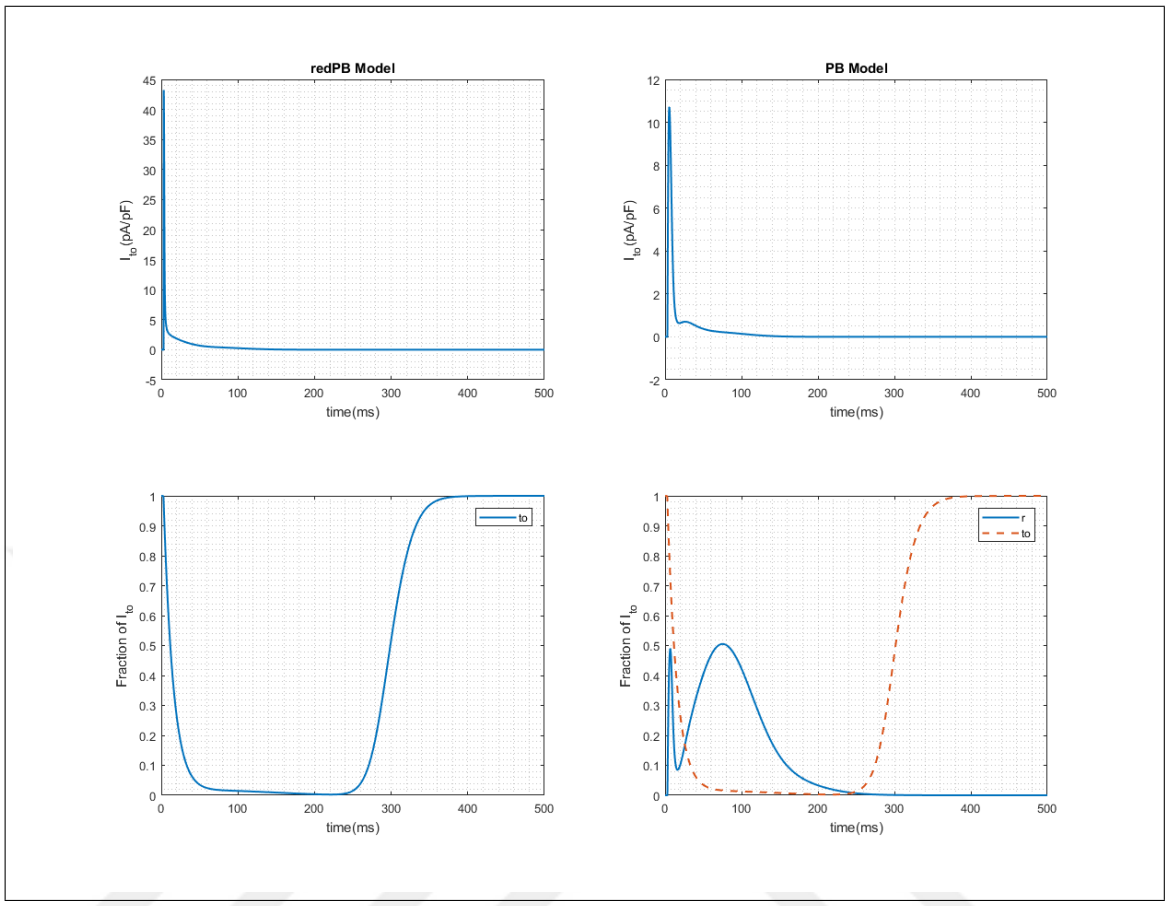

Figure 5.12 Transient outward K^+ current and activation-inactivation variables for redPB and PB models.

5.3.1.4 Delayed Rectifier K^+ Current. K^+ current (I_K) consists of rapid (I_{Kr}) and slow (I_{Ks}) components in the PB model and each of them have a single activation variable. On the other side, the redPB model combines the I_{Ks} and I_{Kr} into a single K^+ current, I_K with single activation variable as shown with Eq. 5.8.

$$I_K = g_K \times X^2 \times (E_m - E_K) \tag{5.8}$$

where g_K is conductance of the channel, E_K is the Nernst potential for delayed rectifier K^+ current, and X is the activation variable.

Simulation results of I_K can be observed in Figure 5.13.

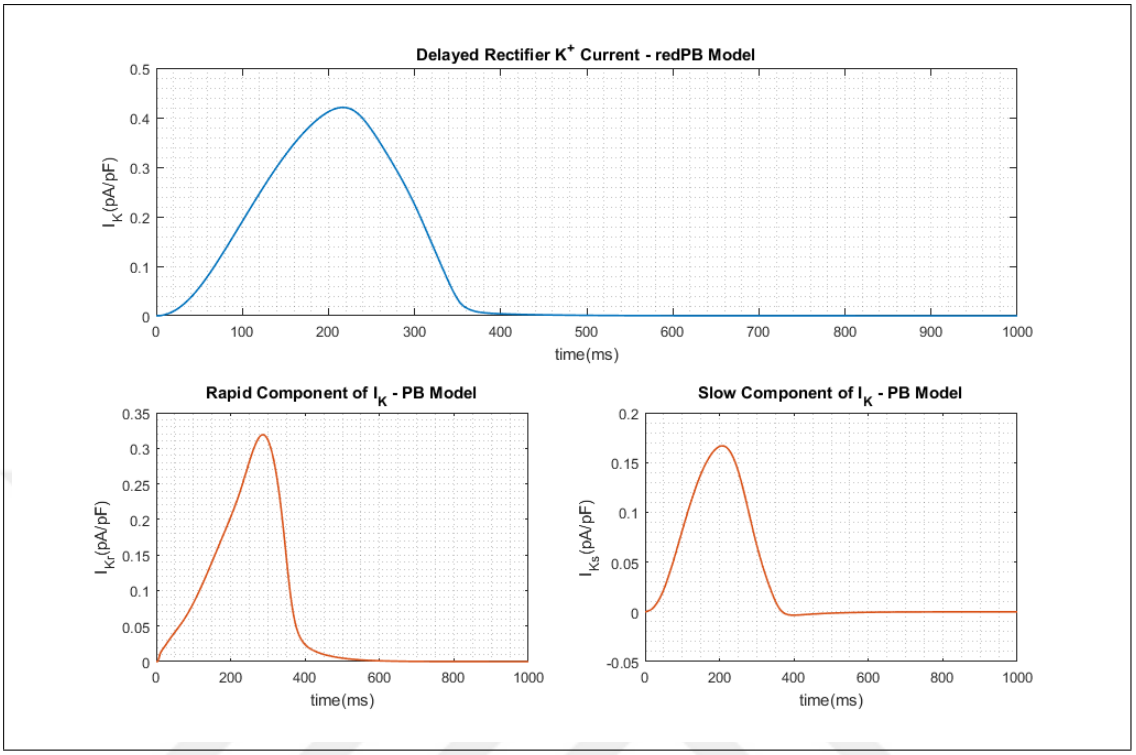

Figure 5.13 Delayed rectifier K^+ current for PB and redPB models.

5.3.2 Heart Failure Case

Severe HF condition may alter the electrical properties of cardiac cells. This situation can induce early or delayed afterdepolarizations which leads to ventricular arrhythmias in these patients. Priebe and Beuckelmann studied the HF condition in their paper using the proposed model. On the other side, there is no information in the literature about the usage of the redPB model for HF condition. In this case, the simulation will be conducted to find out if it is possible to obtain the same HF results using the redPB model.

HF condition leads remodeling of multiple ion channels and alterations of various ionic currents. For instance, potassium channels make a major contribution to repolarization and AP shape formation in cardiac cells. Repolarization abnormalities related to the HF are mostly caused by remodeling-induced changes in potassium cur-

rents. APD prolongation is a consistent feature for the ventricular cells obtained from patients or animals with HF. Potassium channel remodeling is a contributory factor for prolongations in APD. Studies have shown that the HF causes downregulation in transient outward potassium current (I_{to}) and also inward rectifier current (I_{K1}) [64]. Parameter changes related to the currents in the HF condition are shown in Table 5.1. Arrhythmogenic EAD can be promoted through the downregulation of K^+ currents [65].

Table 5.1
Parameters for nonfailing healthy ventricular cells and HF condition in PB model [17].

	Healthy Condition	Diseased Condition
g_{to} $(mS/\mu F)$	0.3	0.191
g_{K1} $(mS/\mu F)$	2.5	2
$g_{Ca,b}$ $(mS/\mu F)$	0.00085	0.0013
$g_{Na,b}$ $(mS/\mu F)$	0.001	0
I_{NaK} (pA/pF)	1.3	0.75
k_{NaCa} (pA/pF)	1000	1650

In the original paper of redPB model, there is no information about parameters to simulate the HF condition. In order to achieve this, parameters are determined to realize the HF using the redPB model. Parameters can be seen in Table 5.2 and the results of the simulation are shown in Figure 5.15.

Table 5.2
Parameters for nonfailing healthy ventricular cells in the redPB model [22]. HF condition paramaters are determined based on the PB model.

	Healthy Condition	Diseased Condition
g_{to} $(mS/\mu F)$	0.4	0.28
g_{K1} $(mS/\mu F)$	3.9	2.2
$g_{Ca,b}$ $(mS/\mu F)$	0.00085	0.001
$g_{Na,b}$ $(mS/\mu F)$	0.001	0
I_{NaK} (pA/pF)	1.3	0.75
k_{NaCa} (pA/pF)	1000	1650

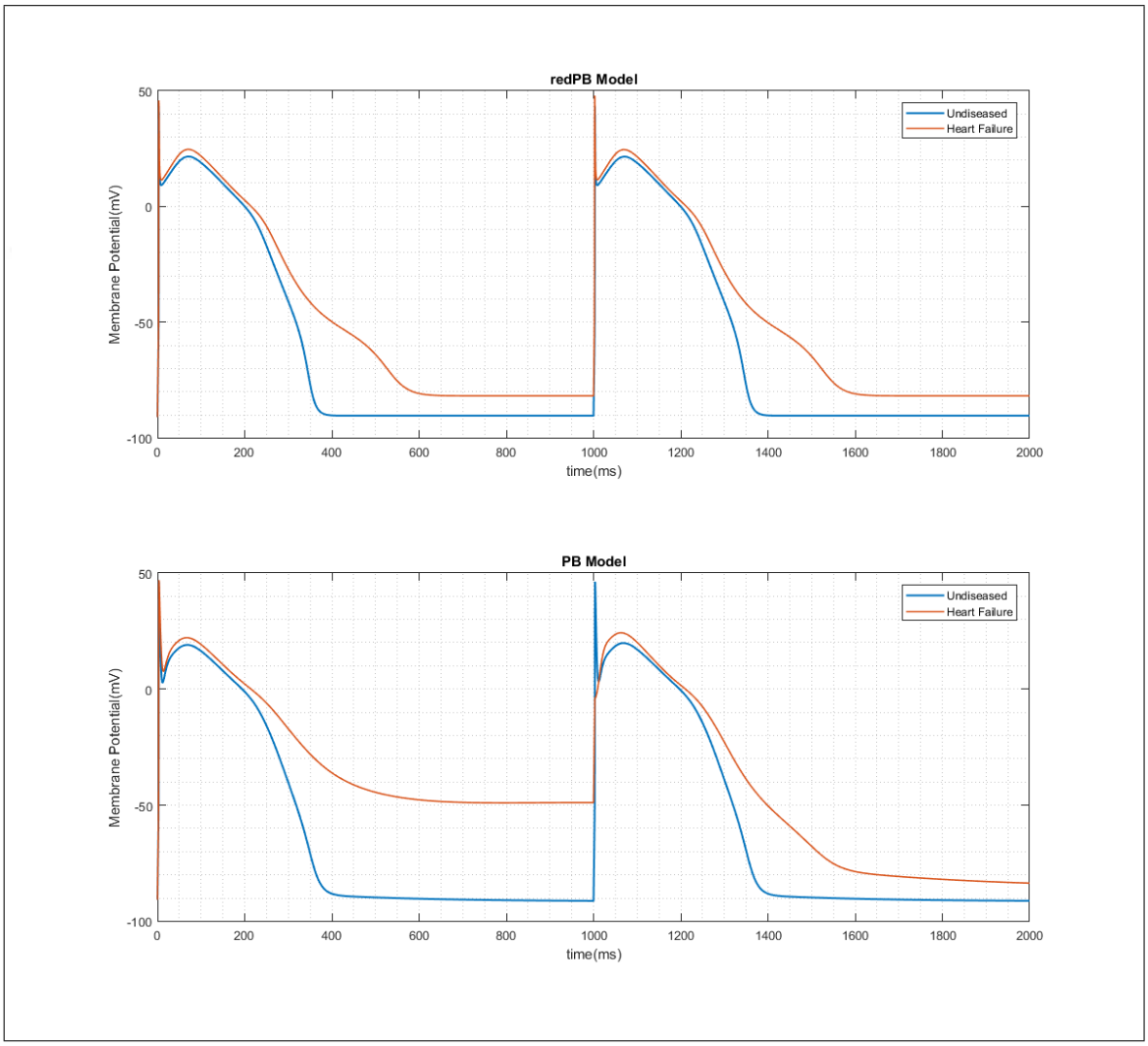

Figure 5.14 Simulation results for undiseased and HF cases using PB and redPB models.

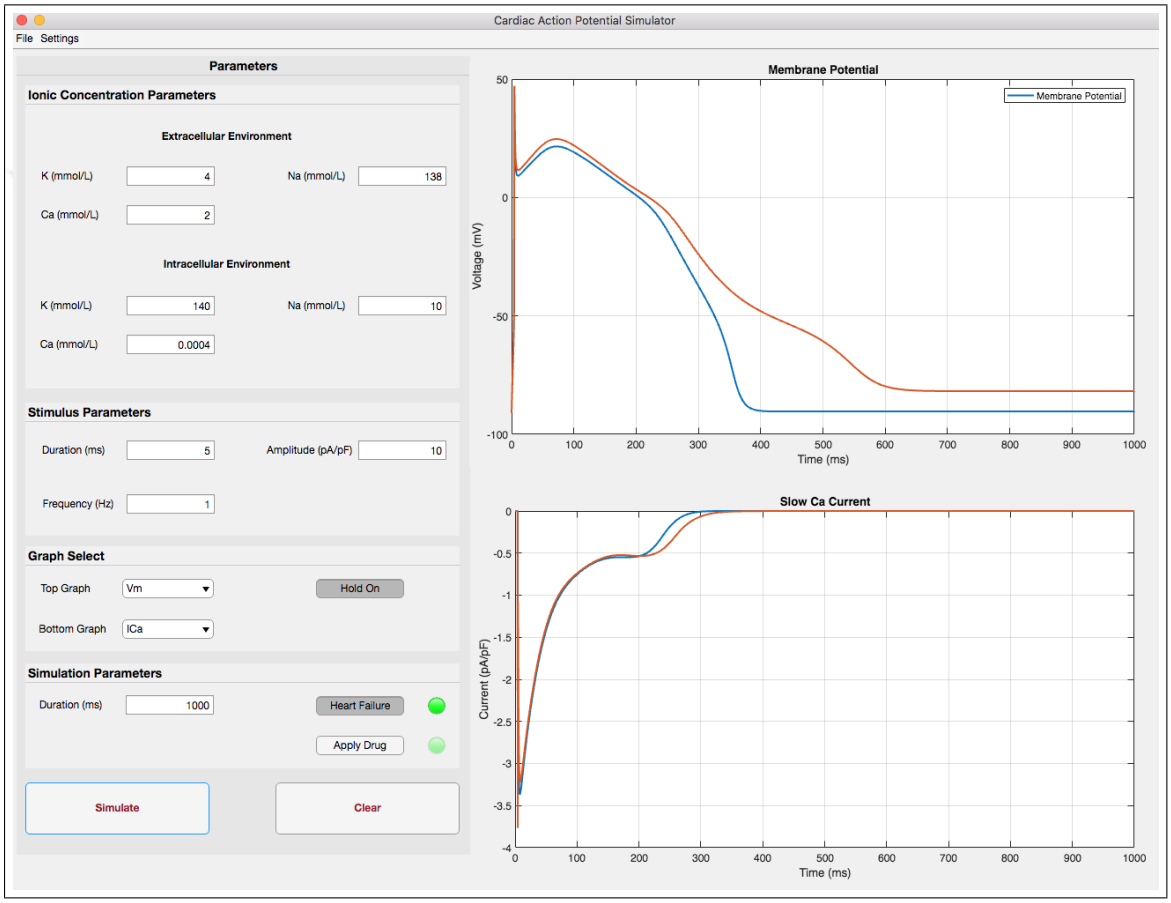

Figure 5.15 Simulation results for undiseased and HF cases on the simulator app GUI developed in MATLAB.

5.3.3 Drug Application

Inhibitory effects of channel blockers are simulated using the PB and the redPB models.

5.3.3.1 Dofetilide. Guo et al. conducted experiments on isolated nonfailing human cardiac cells and observed spontaneous EADs by applying 0,1 μM dofetilide. It blocks rapid component of the delayed rectifier K^+ current (I_{Kr}) approximately at a percentage of 85% as shown in Figure 5.16.

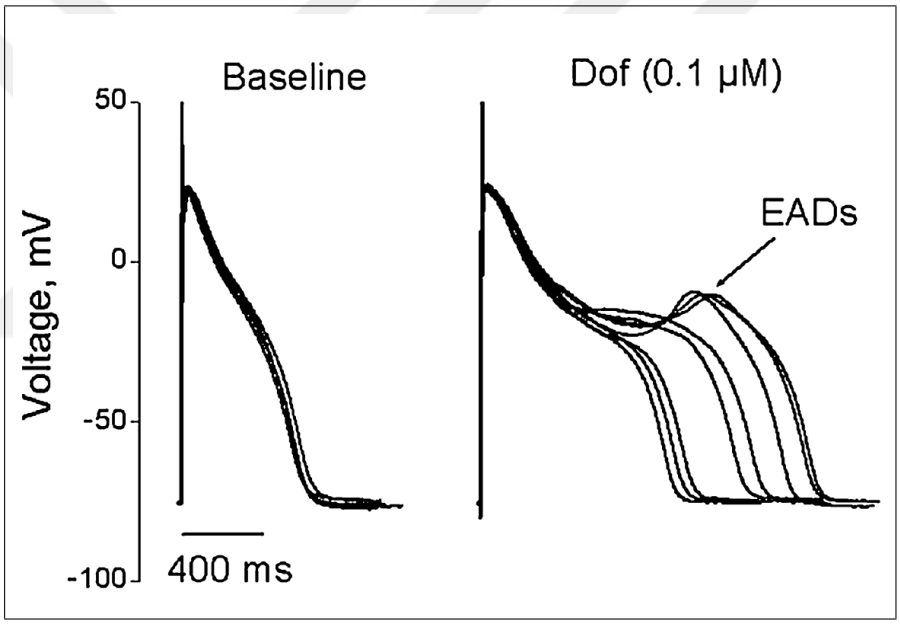

Figure 5.16 Experimental results of dofetilide application to the isolated nonfailing human cardiac cell [16].

The similar drug effect is simulated using the PB model by blocking the I_{Kr} current up to 100%. However, the model failed to generate the same EADs with the experimental results. On the other side, blockage of I_{Kr} left the slow component of delayed rectifier K^+ current (I_{Ks}) alone and ended up with a prolongation in APD by percentage about 50% as shown in Figure 5.17. The redPB model does not contain slow and rapid components of delayed rectifier K^+ current separately. Thus, it is needed to reapply the fitting procedure with blocked values of g_{Kr} and g_{Ks} in order to obtain the new current equation with a drug effect.

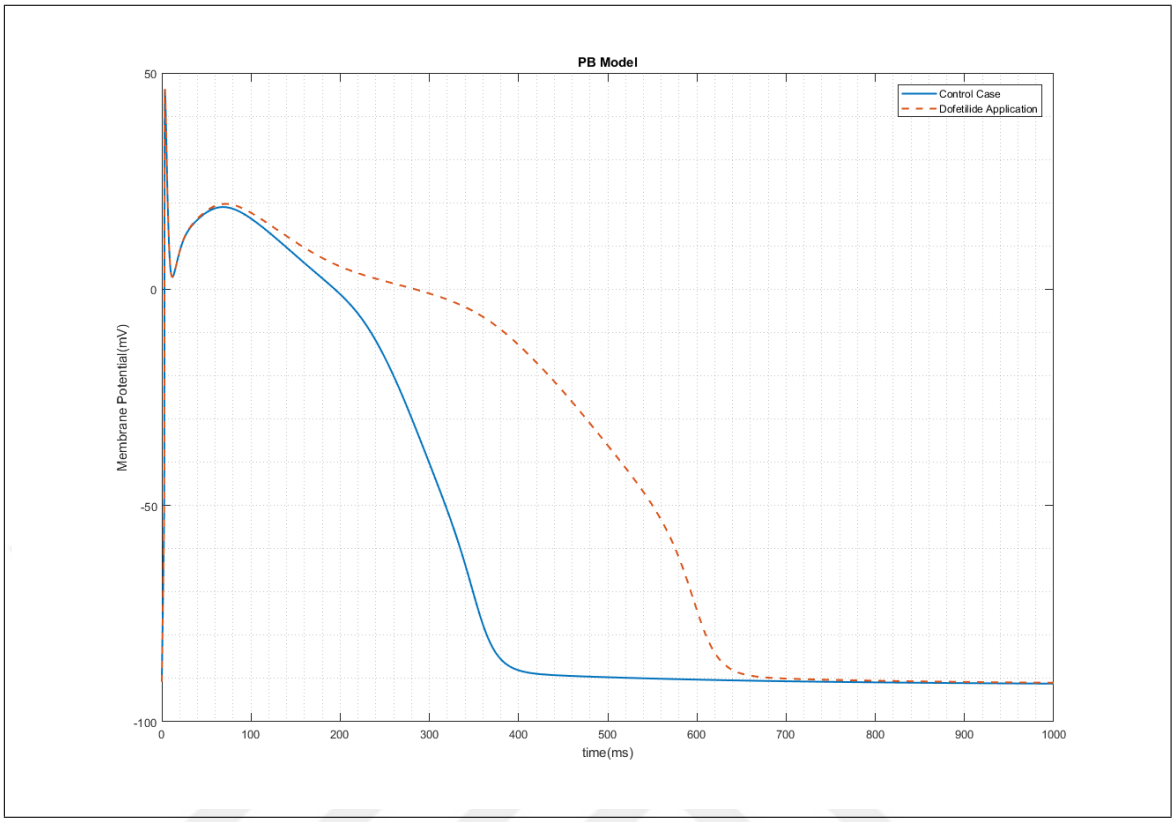

Figure 5.17 Simulation results of dofetilide application using the PB model.

5.3.3.2 4-Aminopyridine (4-AP). It is known that the 4-AP administration prolongs cardiac APD. Hence, a postulation has been made that the APD in cardiac cells may be prolonged through reduction of the transient outward K^+ current (I_{to}). On the other side, 4-AP also has additional effects on the other ionic currents especially Ca^{2+} current and delayed rectifier K^+ current. Priebe and Beuckelmann assessed the I_{to} inhibition effect of 4-AP on the APD in human ventricular cells [17].

Figure 5.18 shows that several degrees of I_{to} current inhibition (25%, 50%, 75%, and 100%) nearly does not affect the APD in nonfailing human ventricular cells.

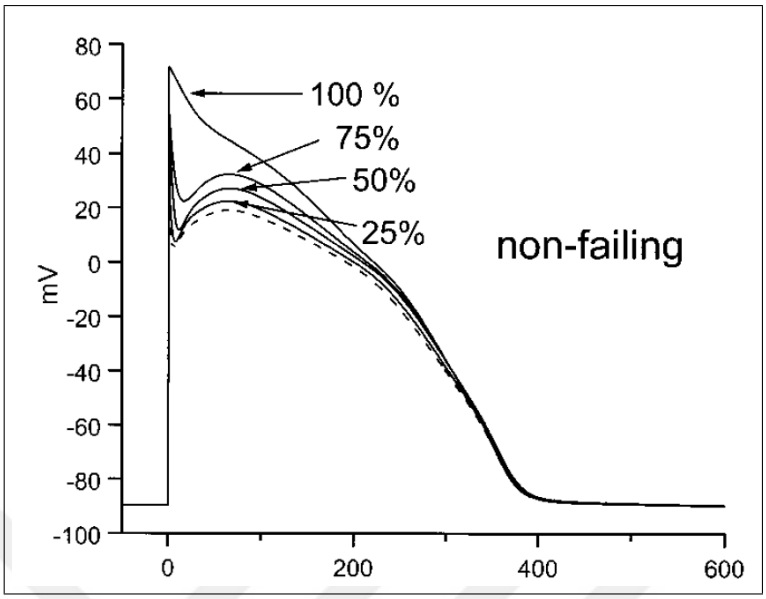

Figure 5.18 Various degrees of I_{to} inhibition by application of 4-AP [17].

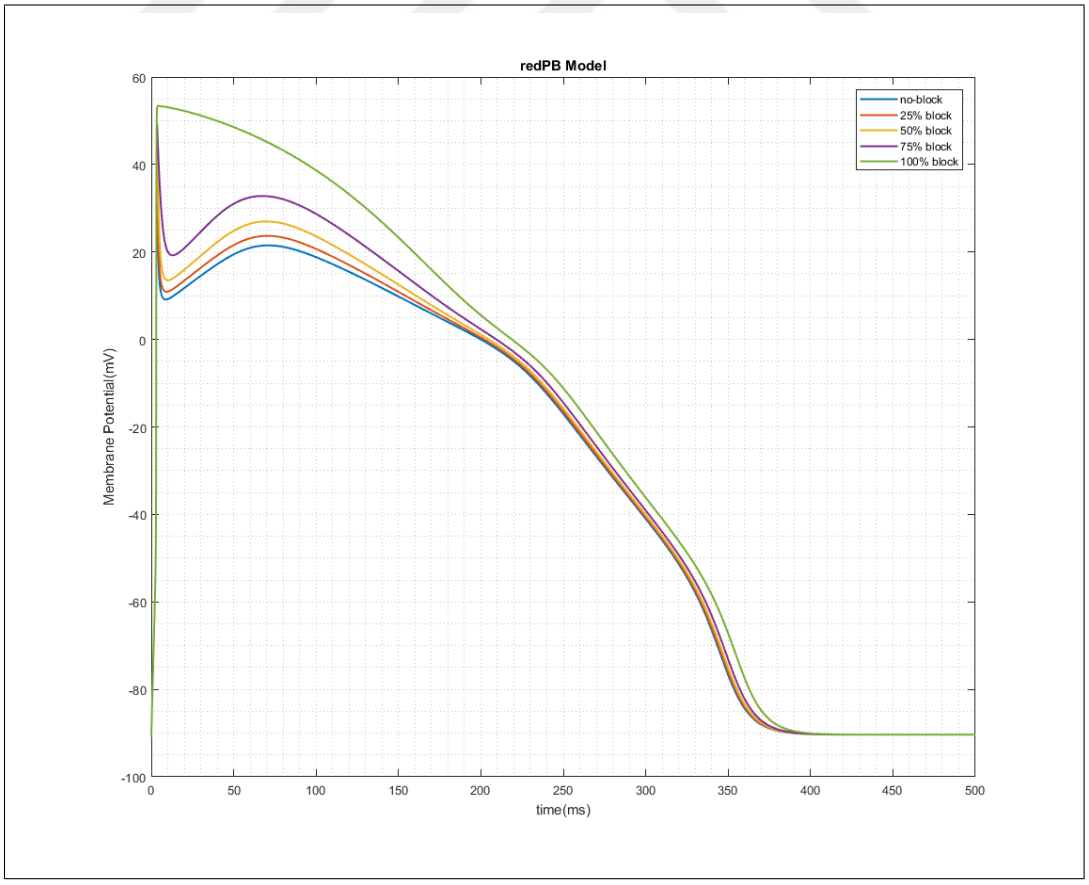

Figure 5.19 Simulation results of 4-AP application using the redPB model.

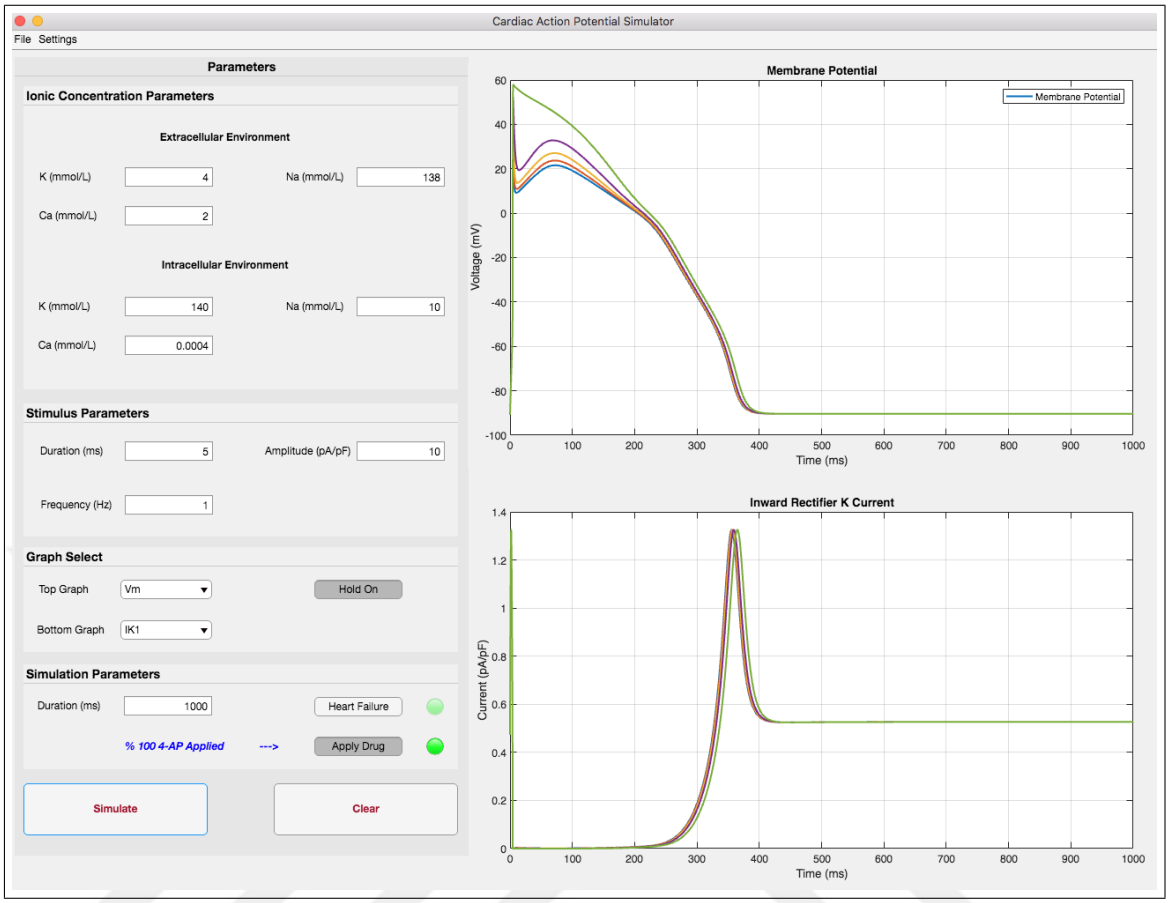

Figure 5.20 Simulator view of the 4-AP drug application case. Various degrees of I_{to} inhibitions can be seen, no-block, 25% block, 50% block, 75% block, and full block from bottom to top, respectively.

6. SUMMARY AND CONCLUSIONS

6.1 Discussions

Consequences of the HF condition were studied using the PB model in the original paper published by Priebe and Beuckelmann. However, although the redPB model is more stable and computationally more effective in comparison with the PB model, it was not used to study the HF consequences before. The reason may be that the redPB model lacks calcium handling mechanism descriptions and contains fixated intracellular ion concentrations. Nevertheless, parameters of the redPB model are adjusted to observe the effects of the HF on the ventricular AP. As a result, it is shown that the duration and shape of the AP generated using the redPB model under the HF condition is almost the same with the HF simulation conducted using the PB model. Thus, the ventricular AP shape of the failing heart is generated 29% faster by using the redPB model than using the PB model.

Priebe and Beuckelmann simulated the transient outward K^+ current inhibition effect of 4-AP administration using their model in the original paper. 4-AP is known to prolong the APD. However, the simulation results showed that the APD did not change with the inhibition of I_{to} up to 100%. This may be due to the compensative effect of the other currents especially I_{Ca} and I_K. The same conditions simulated using the redPB model in this thesis and the obtained results were the same with the Priebe and Beuckelmann's.

Experimental results claim that the dofetilide blocks the delayed rectifier K^+ current's rapid component and may lead spontaneous EADs on the ventricular AP. The inhibition effect of 0,1 μM dofetilide is simulated using the PB model for nonfailing human ventricular cells. Based on the simulation results, the APD prolonged up to 50%, however, EADs did not occur. Priebe and Beuckelmann claimed that the EADs occur when the rapid component of the delayed rectifier K^+ current is reduced by

75% for the failing ventricular cells. These conditions could not be simulated using the redPB model due to the fact that it contains single delayed rectifier K^+ current instead of rapid and slow components.

6.2 Conclusions and Recommendations for Future Work

In the field of computational modeling of the cardiac electrophysiology, this thesis has been mainly focused on simulation platform development to run the existing cardiac cell models in a user-friendly and effective manner.

Firstly, simulation software is written in Python with a user-friendly GUI design. Several cardiac cell models which already exist in the CellML format can be converted to the mmt file format so as to be used with this software. The user can easily edit/modify the mmt model file in any text editor and import it to the software in order to conduct simulations using it thanks to the Myokit Python API. The main window of the software allows editing just the basic parameters related to the imported cardiac cell model for the purpose of hiding the model complexity from the user as much as possible. The further parameters can be adjusted through the parameters window of the software or by editing the model file in a text editor prior to importation. The mmt model file is created based on the PB model for the human ventricular cell. Subsequently, the model file is imported to the software and the simulation is conducted with the basic parameters. As a result of the simulation, the ventricular action potential shape and the related ionic current graphs are successfully reproduced for nonfailing and failing human ventricular cells as claimed in the original paper of model description.

Secondly, a cardiac action potential simulator application is developed by using the MATLAB App Designer. The reduced version of the PB model, redPB model, is implemented to the application and the basic parameters of the model are allowed to be adjusted through a user-friendly GUI. The ventricular action potential shape and the related ionic current graphs are successfully reproduced through the application

in comparison with the original redPB model paper. Moreover, drug administration feature is added to the application in order to observe the effects of the channel blocker drugs on the ventricular AP.

Computational models of the cardiac cells provide significant opportunity to investigate the cardiac electrophysiology at cellular and subcellular levels through conducting *in silico* simulations. The modern cardiac cell models contain a high degree of physiological details which means a large number of differential equations and variables. Thus, easy-to-use simulation platforms are needed for using these models without any coding knowledge is required. Currently, there are a few platforms developed for this purpose such as OpenCOR and OpenCell. On the other side, they are not dedicated platforms for cardiac cell simulations and it can be tedious to edit the model files in XML format. The main aim of this thesis was to develop easy-to-use simulation platforms with user-friendly GUIs for human ventricular cell models. MATLAB based application is developed for this purpose and the redPB model is implemented. A user-friendly GUI is designed thanks to the MATLAB's brand new application development tool named App Designer. Model importation feature can be added as future work in order to allow simulations using the other models. Furthermore, a MATLAB based model description language can be developed in order to utilize the computational power of MATLAB and make the cardiac cell models more accessible for the wide user community of it. The drug administration panel is implemented in order to allow drug based simulations. Different drug types can be added to the application as future work.

Additionally, a more comprehensive cardiac action potential simulator is written in Python as standalone computer software which allows user import a variety of cardiac cell models and conduct simulations using them. The software accepts the mmt file format which is much easier to edit/modify in comparison with the XML based model files. Drug administration feature can be added as future work. Furthermore, an online repository can be designed to add a variety of cardiac cell models in mmt file format. Hence, the user can remotely connect to the repository and fetch any model to conduct simulations through the software.

A vast majority of the cardiac cell models have been developed on the basis of the Hodgkin-Huxley formalism. Hodgkin and Huxley utilized variable resistor to model the current and membrane potential relationship of the ion channels. However, in point of fact, ion channels of the excitable cell membranes have a non-linear exponential current relationship to the electrical potential on the cell membrane. This kind of relationship cannot be truly realized using resistors and through linearized conductance [66]. Instead, semiconductors such as MOSFETs are more appropriate to model the non-linear exponential characteristics of the transmembrane ion channels due to their inherent non-linear channel characteristics. Thus, a novel MOSFET based cardiac cell model can be developed as future work.

REFERENCES

1. Sigg, D. C., P. A. Iaizzo, Y.-F. Xiao, and B. He, *Cardiac Electrophysiology Methods and Models*, Springer Science & Business Media, 2010.

2. Martini, F., J. L. Nath, and E. F. Bartholomew, *Fundamentals of Anatomy & Physiology*, Pearson, 2015.

3. Chang, E. T.-Y., *Towards Understanding the Electrogram: Theaoretical & Experimental Multiscale Modelling of Factors Affecting Action Potential Propagation in Cardiac Tissue*, Imperial College London, 2013.

4. Iaizzo, P. A., *Handbook of Cardiac Anatomy, Physiology, and Devices*, Springer Science & Business Media, 2009.

5. Ikonnikov, G., and D. Yelle, *Physiology af Cardiac Conduction and Contractility*, McMaster Pathophysiology Review (MPR), 2018. Available: http://www.pathophys.org.

6. Jost, N., "Transmembrane ionic currents underlying cardiac action potential in mammalian hearts," *Advances in cardiomyocyte research*, pp. 1–45, 2009.

7. Tortora, G. J., and B. H. Derrickson, *Principles of Anatomy and Physiology*, John Wiley & Sons, 2008.

8. Liang, W., Y. Zhao, L. Liu, Y. Wang, W. J. Li, and G.-B. Lee, "Determination of cell membrane capacitance and conductance via optically induced electrokinetics," *Biophysical journal*, Vol. 113, no. 7, pp. 1531–1539, 2017.

9. Guo, T., A. Al Abed, N. H. Lovell, and S. Dokos, "A generic ionic model of cardiac action potentials," in *2010 Annual International Conference of the IEEE Engineering in Medicine and Biology*, pp. 1465–1468, IEEE, 2010.

10. Doi, S., J. Inoue, Z. Pan, and K. Tsumoto, *Computational Electrophysiology*, Vol. 2, Springer Science & Business Media, 2010.

11. Hodgkin, A. L., and A. F. Huxley, "A quantitative description of membrane current and its application to conduction and excitation in nerve," *The Journal of physiology*, Vol. 117, no. 4, pp. 500–544, 1952.

12. Katz, A. M., *Physiology of the Heart*, Lippincott Williams & Wilkins, 2010.

13. Noble, D., "A modification of the hodgkin huxley equations applicable to purkinje fibre action and pacemaker potentials," *The Journal of physiology*, Vol. 160, no. 2, pp. 317–352, 1962.

14. *Priebe - Beuckelmann Model*, Physiome Model Repository, 1998. Available: https://models.physiomeproject.org/exposure/.

15. *Bernus et al. Model*, Physiome Model Repository, 2002. Available: https://models.physiomeproject.org/e/5/view.

16. Guo, D., Q. Liu, T. Liu, G. Elliott, M. Gingras, P. R. Kowey, and G.-X. Yan, "Electrophysiological properties of hbi-3000: a new antiarrhythmic agent with multiple-channel blocking properties in human ventricular myocytes," *Journal of cardiovascular pharmacology*, Vol. 57, no. 1, pp. 79–85, 2011.

17. Priebe, L., and D. J. Beuckelmann, "Simulation study of cellular electric properties in heart failure," *Circulation research*, Vol. 82, no. 11, pp. 1206–1223, 1998.

18. Clerx, M. P. É., *Multi-Scale Modeling and Variability in Cardiac Cellular Electrophysiology*, Maastricht University, 2017.

19. Katz, A. M., "Cardiac ion channels," *New England Journal of Medicine*, Vol. 328, no. 17, pp. 1244–1251, 1993.

20. Macfarlane, P. W., A. Van Oosterom, O. Pahlm, P. Kligfield, M. Janse, and J. Camm, *Comprehensive Electrocardiology*, Springer Science & Business Media, 2010.

21. Noble, D., A. Garny, and P. J. Noble, "How the hodgkin–huxley equations inspired the cardiac physiome project," *The Journal of physiology*, Vol. 590, no. 11, pp. 2613–2628, 2012.

22. Bernus, O., R. Wilders, C. W. Zemlin, H. Verschelde, and A. V. Panfilov, "A computationally efficient electrophysiological model of human ventricular cells," *American Journal of Physiology-Heart and Circulatory Physiology*, Vol. 282, no. 6, pp. H2296–H2308, 2002.

23. Benjamin, E. J., P. Muntner, A. Alonso, and et al., "Heart disease and stroke statistics - 2019 update: A report from the american heart association," *Circulation*, Vol. 139, no. 10, pp. e56–e528, 2019.

24. Wilkins, E., L. Wilson, K. Wickramasinghe, P. Bhatnagar, J. Leal, R. Luengo-Fernandez, R. Burns, M. Rayner, and N. Townsend, "European cardiovascular disease statistics 2017," 2017.

25. "Ölüm nedeni istatistikleri 2017," *Türkiye İstatistik Kurumu Haber Bülteni*, no. 27620, 2018.

26. *Cardiovascular Diseases (CVDs)*, World Health Organization, 2017. Available: https://www.who.int/news-room/fact-sheets/detail/cardiovascular-diseases-(cvds).

27. Gheorghe, A., U. Griffiths, A. Murphy, H. Legido-Quigley, P. Lamptey, and P. Perel, "The economic burden of cardiovascular disease and hypertension in low-and middle-income countries: a systematic review," *BMC public health*, Vol. 18, no. 1, p. 975, 2018.

28. Olivetti, G., G. Giordano, D. Corradi, M. Melissari, C. Lagrasta, S. R. Gambert, and P. Anversa, "Gender differences and aging: effects on the human heart," *Journal of the American College of Cardiology*, Vol. 26, no. 4, pp. 1068–1079, 1995.

29. Anumonwo, J. M., and S. V. Pandit, "Ionic mechanisms of arrhythmogenesis," *Trends in cardiovascular medicine*, Vol. 25, no. 6, pp. 487–496, 2015.

30. Cutler, M. J., D. Jeyaraj, and D. S. Rosenbaum, "Cardiac electrical remodeling in health and disease," *Trends in pharmacological sciences*, Vol. 32, no. 3, pp. 174–180, 2011.

31. Billman, G. E., *Novel Therapeutic Targets for Antiarrhythmic Drugs*, John Wiley & Sons, 2010.

32. Ten Tusscher, K. H., O. Bernus, A. V. Panfilov, *et al.*, "Comparison of electrophysiological models for human ventricular cells and tissues," *Progress in biophysics and molecular biology*, Vol. 90, no. 1-3, pp. 326–345, 2006.

33. Noble, D., "Successes and failures in modeling heart cell electrophysiology," *Heart Rhythm*, Vol. 8, no. 11, pp. 1798–1803, 2011.

34. Puglisi, J. L., and D. M. Bers, "Labheart: an interactive computer model of rabbit ventricular myocyte ion channels and ca transport," *American Journal of Physiology-Cell Physiology*, Vol. 281, no. 6, pp. C2049–C2060, 2001.

35. Scanlon, V. C., and T. Sanders, *Essentials of Anatomy and Physiology*, FA Davis, 2014.

36. Cook, M. S., K. P. Roberts, and A. J. Weinhaus, "Anatomy of the thoracic wall, pulmonary cavities, and mediastinum," in *Handbook of Cardiac Anatomy, Physiology, and Devices*, pp. 33–58, Springer, 2009.

37. Silbernagl, S., A. Despopoulos, W.-R. Gay, A. Rothenburger, and S. O. Wandrey, *Color Atlas of Physiology*, Vol. 5, Thieme Stuttgart, 2009.

38. Barrio, R., I. Domınguez, M. Quiroz-Juárez, O. Jiménez-Ramırez, R. Vázquez-Medina, and J. Aragón, "Modelling the electrical activity of the heart," *World Scientific*, Vol. 6, no. 09, p. 2017, 2018.

39. Waller, B., L. Gering, N. Branyas, and J. Slack, "Anatomy, histology, and pathology of the cardiac conduction system: Part i.," *Clinical cardiology*, Vol. 16, no. 3, pp. 249–252, 1993.

40. Kahle, W., H. Leonhardt, and W. Platzer, *Color Atlas and Textbook of Human Anatomy. Vol. 2: Internal Organs*, Thieme Medical Publishers, 2007.

41. Van De Graaff, K. M., *Human Anatomy, Wm. C*, Brown Publishers, Melbourne, 1995.

42. Ho, S. Y., *Anatomy for Cardiac Electrophysiologists: A Practical Handbook*, Cardiotext publishing, 2012.

43. Sterratt, D. C., *Goldman-Hodgkin-Katz Equations*, pp. 1–3. New York, NY: Springer New York, 2013.

44. Sembulingam, K., and P. Sembulingam, *Essentials of Medical Physiology*, JP Medical Ltd, 2012.

45. Eisner, D. A., J. L. Caldwell, K. Kistamás, and A. W. Trafford, "Calcium and excitation-contraction coupling in the heart," *Circulation research*, Vol. 121, no. 2, pp. 181–195, 2017.

46. Douglas, P. Z., and J. Jalife, *Cardiac Electrophysiology: From Cell to Beside*, Saunders Elsevier, 2009.

47. Ono, K., and T. Iijima, "Cardiac t-type calcium channels in the heart," *Journal of molecular and cellular cardiology*, Vol. 48, no. 1, pp. 65–70, 2010.

48. Balser, J. R., "Structure and function of the cardiac sodium channels," *Cardiovascular research*, Vol. 42, no. 2, pp. 327–328, 1999.

49. Potse, M., "Mathematical modeling and simulation of ventricular activation sequences: implications for cardiac resynchronization therapy," *Journal of cardiovascular translational research*, Vol. 5, no. 2, pp. 146–158, 2012.

50. DiMasi, J. A., R. W. Hansen, and H. G. Grabowski, "The price of innovation: new estimates of drug development costs," *Journal of health economics*, Vol. 22, no. 2, pp. 151–185, 2003.

51. Van Der Pol, B., and J. Van Der Mark, "The heartbeat considered as a relaxation oscillation, and an electrical model of the heart," *The London, Edinburgh, and Dublin Philosophical Magazine and Journal of Science*, Vol. 6, no. 38, pp. 763–775, 1928.

52. Britain, R. S. G., *Biographical Memoirs of Fellows of the Royal Society*, Royal Society, 1992.

53. Cronin, J., *Mathematical Aspects of Hodgkin-Huxley Neural Theory*, Vol. 7, Cambridge University Press, 1987.

54. Heitler, W. J., *The Hodgkin-Huxley Model for the Generation of Action Potentials*, University of St Andrews, 2007. Available: https://www.st-andrews.ac.uk/ wjh/.

55. Noble, D., "From the hodgkin–huxley axon to the virtual heart," *The Journal of physiology*, Vol. 580, no. 1, pp. 15–22, 2007.

56. O'Hara, T., L. Virág, A. Varró, and Y. Rudy, "Simulation of the undiseased human cardiac ventricular action potential: model formulation and experimental validation," *PLoS computational biology*, Vol. 7, no. 5, p. e1002061, 2011.

57. Aithal, H., O. Kumar, and M. R. Narasimhan, "Introducing complex software design in matlab via enterprise architect," in *2016 IEEE International Conference on Engineering and Technology (ICETECH)*, pp. 981–983, IEEE, 2016.

58. Smith, S. T., *MATLAB: Advanced GUI Development*, Dog ear publishing, 2006.

59. Oliphant, T. E., "Python for scientific computing," *Computing in Science & Engineering*, Vol. 9, no. 3, pp. 10–20, 2007.

60. Cass, S., and B. Parthasaradhi, "Interactive: The top programming languages 2018," *IEEE Spectrum*, 2018.

61. Sanner, M. F., *et al.*, "Python: a programming language for software integration and development," *J Mol Graph Model*, Vol. 17, no. 1, pp. 57–61, 1999.

62. Clerx, M., P. G. Volders, and P. Collins, "Myokit: A framework for computational cellular electrophysiology," in *Computing in Cardiology 2014*, pp. 229–232, IEEE, 2014.

63. Lei, C. L., K. Wang, M. Clerx, R. H. Johnstone, M. P. Hortigon-Vinagre, V. Zamora, A. Allan, G. L. Smith, D. J. Gavaghan, G. R. Mirams, *et al.*, "Tailoring mathematical models to stem-cell derived cardiomyocyte lines can improve predictions of drug-induced changes to their electrophysiology," *Frontiers in physiology*, Vol. 8, p. 986, 2017.

64. Rahm, A.-K., P. Lugenbiel, P. A. Schweizer, H. A. Katus, and D. Thomas, "Role of ion channels in heart failure and channelopathies," *Biophysical reviews*, Vol. 10, no. 4, pp. 1097–1106, 2018.

65. Nattel, S., A. Maguy, S. Le Bouter, and Y.-H. Yeh, "Arrhythmogenic ion-channel remodeling in the heart: heart failure, myocardial infarction, and atrial fibrillation," *Physiological reviews*, Vol. 87, no. 2, pp. 425–456, 2007.

66. Farquhar, E., and P. Hasler, "A bio-physically inspired silicon neuron," *IEEE Transactions on Circuits and Systems I: Regular Papers*, Vol. 52, no. 3, pp. 477–488, 2005.